Ni
10 Co
8 Cr
6 Mo
6 Al
4 Ta
1 Ti
+ C
+ Zr
+ B

B-1900

## GENERAL

B-1900 is a cast nickel-base alloy developed by Pratt and Whitney Aircraft in their search for alloys exhibiting high strength at temperatures in the range of 1900 F while still exhibiting a creep ductility above 1 percent at 1400 F, where other nickel-base alloys become embrittled. B-1900 is covered by U.S. Patent No. 3,310,399 to which United Aircraft Corporation has exclusive rights. Its good thermal fatigue resistance has resulted in its use in turbine airfoils where temperatures and thermal gradients are high. An aluminized coating is normally required to impart oxidation resistance for this application. Although the alloy can be used in the as-cast condition, an aging treatment is commonly applied to improve ductility and notch creep strength. The alloy has also been produced in the directionally solidified form with some improvement in creep resistance at high temperature. The addition of hafnium produces major increases in the 1400 F creep ductility as well as thermal fatigue resistance. The addition of silicon has also been found to improve oxidation resistance but impairs rupture life and ductility. Close control of bismuth and lead content is necessary for high temperature strength and ductility, as is the case with other high strength nickel-base alloys.

1.01 **Commercial Designation**
B-1900.

1.02 **Alternate Designations**
PWA 663 is Pratt and Whitney's designation for B-1900. PWA 1455 is a variation containing 1.4 percent hafnium. Also Austenal B-1900 and Udimet B-1900.

1.03 **Specifications**
PWA 663 and PWA 1455 as described in Section 1.02.

1.04 **Composition**
Composition, Table 1.04.

1.05 **Heat Treatment**
Alloy may be used in as-cast condition.

1.051 For improvement in rupture life and ductility at 1400 F heat treat as indicated in Section 1.0511.

1.0511 Heat to 1975 ± 25 F in air, 4 hr, air cool; age at 1650 ± 25 F 10 hr, air cool. The 1975 F treatment is usually accomplished during the coating process.

1.06 **Hardness**

1.061 After heat treatment (Section 1.0511), Rockwell C hardness range should be 34-44.

1.062 Effect of time and temperature of exposure on room temperature hardness, Figure 1.062.

1.07 **Forms and Conditions Available**

1.071 Alloy is cast to shape. Principal use is turbine blades and vanes.

1.072 Directionally solidified test specimens and turbine blades and vanes have been produced.

1.08 **Melting and Casting Practice**

1.081 Master heat cast under vacuum.

1.082 Castings are produced from master heat ingot, remelted and poured under vacuum without loss of vacuum between melting and pouring. Casting in argon produces superior strength and ductility at temperatures below 1400 F, but above 1600 F, vacuum casting produces higher properties.

1.083 Revert shall not be remelted directly for pouring of castings; it may be used in preparation of master heats.

1.09 **Special Considerations**

1.091 Alloy PWA 1455 containing hafnium has higher shrinkage characteristics than conventional alloy PWA 663; therefore, it requires special gating and pouring practice relative to similar parts made from alloy PWA 663.

1.092 Considerable improvement in oxidation resistance has been achieved by silicon additions (Figures 2.0314 and 2.0315). Sulfidation resistance is also improved by silicon addition (Figure 2.0327). However, the mechanical properties may be adversely affected. (See Figures 3.0316, 3.0434, and 3.0435).

1.093 Lead content is very critical to creep rupture properties (Figure 3.0436).

1.094 Standard castings normally contain up to 1 percent porosity, with higher porosity in thick sections than in thin sections. (See Figure 1.0941.) Porosity can be reduced by solidification under pressurized argon (34) or by hot isostatic pressing (HIP) after casting, with resultant improvement in mechanical properties. (See Figures 3.0461, 3.0462, and 3.0514.)

1.0941 Number of measurements at various porosity percentages for cast turbine blade airfoil and root sections, Figure 1.0941.

## 2 PHYSICAL AND CHEMICAL PROPERTIES

2.01 **Thermal Properties**

2.011 Melting range, 2325–2375 F (4) and 2318–2372 F (35) reported for standard alloy; 2345–2381 F (36) reported for B-1900 + 1.4 percent hafnium.

2.012 Phase changes.

2.0121 Minor phase concentration for alloy at various times and temperatures, Figure 2.0121.

2.0122 Minor phase concentration for alloy at long exposure times from 1400 to 2100 F, Figure 2.0122.

2.0123 Effect of exposure time and temperature on the $M_6C$ phase, Figure 2.0123.

2.0124 Effect of exposure time and temperature on the MC phase, Figure 2.0124.

2.0125 Effect of exposure time and temperature on the $M_{23}C_6$ phase, Figure 2.0125.

2.013 Thermal conductivity, Figure 2.013.

2.014 Thermal expansion, Figure 2.014

2.015 Specific heat, Figure 2.015.

2.016 Thermal diffusivity, 0.182 $ft^2/hr$ (2).

2.02 **Other Physical Properties**

2.021 Density, 0.297 $lb/in.^3$; 8.22 $gm/cm^3$.

2.022 Electrical properties.

2.023 Magnetic properties.

2.024 Emittance.

2.025 Damping capacity.

Ni
10 Co
8 Cr
6 Mo
6 Al
4 Ta
1 Ti
+ C
+ Zr
+ B

B-1900

2.03 **Chemical Properties**

2.031 Oxidation. B-1900 has very good oxidation resistance in air or oxygen. It is an alumina-former in that the thin scale formed during oxidation in static or slowly flowing air or oxygen is primarily $Al_2O_3$, with some dissolved $TiO_2$. A minor fraction of the surface forms chromia, with internal alumina "fingers" underneath. The oxidation weight gains are approximately proportional to the logarithm of exposure time (Figure 2.0311), although loss of volatile $CrO_3$ above 1700 F causes deviations from the logarithmic rate law at long times (37).

2.0311 Oxidation kinetics of alloy. Figure 2.0311.

2.0312 Static air oxidation under isothermal and cyclic conditions at 2000 F with comparison to Inconel 713C, another nickel-base alloy. Figure 2.0312.

2.0313 High velocity (Mach 1) oxidation under isothermal and cyclic conditions at 2000 F with comparison to Inconel 713C, another nickel-base alloy. Figure 2.0313.

2.0314 Effect of silicon concentration on isothermal oxidation at 2012 and 2192 F. Figure 2.0314.

2.0315 Effect of cycle period and silicon concentration on cyclic furnace oxidation. Figure 2.0315.

2.0316 Effect of temperature on life of coating subjected to high velocity (Mach 0.8) combustion jet. Figure 2.0316.

2.032 Hot corrosion. This accelerated type of oxidation-corrosion is caused by the presence of $Na_2SO_4$ (m.p. 1620 F), which fluxes the otherwise protective scale and causes rapid and sometimes catastrophic oxidation. The alumina-rich scale which normally forms on B-1900 is particularly prone to hot corrosion, producing oxidation rates as much as several magnitudes greater than in the absence of $Na_2SO_4$ (Figure 2.0321). In actual service, hot corrosion is caused by reaction of ingested NaCl (from marine atmospheres) with sulfur contaminant in the fuel (Figures 2.0322 and 2.0323). Chromia on the alloy surface reduces susceptibility to hot corrosion (Figure 2.0324). Higher chromium contents or higher Cr/Al ratios in other superalloys also reduce the severity and increase the threshold temperature for hot corrosion by promoting chromia-rich oxide scales (Figures 2.0325 and 2.0326). Molybdenum is considered to promote hot corrosion, while tantalum may reduce it (Figure 2.0328).

2.0321 Effect of precoating with $Na_2SO_4$ on hot corrosion weight gain in slowly flowing oxygen at 1832 F. Figure 2.0321.

2.0322 Corrosion (as measured by depth of attack) for alloy in 700 fps velocity gas jet using low sulfur fuel (JP-4) with 4 ppm and 8 ppm sea salt in inlet air. Figure 2.0322.

2.0323 Corrosion (as measured by depth of attack) for alloy in 700 fps velocity gas jet using high sulfur fuel (JP-4R) with 4 ppm and 8 ppm sea salt in inlet air. Figure 2.0323.

2.0324 Effect of chromia additives on sulfidation of alloy at 1742 F. Figure 2.0324.

2.0325 Correlation showing that low corrosion resistance of alloy is related to its low chromium content. Figure 2.0325.

2.0326 Correlation showing that the low threshold temperature for corrosion is principally related to its chromium content. Figure 2.0326.

2.0327 Effect of silicon concentration on resistance to hot corrosion in Mach 1 burner exhaust and comparison with aluminide-coated specimen. Figure 2.0327.

2.0328 Effect of substituting tantalum for molybdenum on hot corrosion behavior at 1652 F in slowly flowing oxygen. Figure 2.0328.

2.04 **Nuclear Properties**

3 **MECHANICAL PROPERTIES**

3.01 **Specified Mechanical Properties**

Specified mechanical properties. Table 3.01.

3.02 **Mechanical Properties at Room Temperature**

3.021 Tension.

3.0211 Stress-strain curves for as-cast alloy. Figure 3.0211.

3.0212 Stress-strain curves for heat treated alloy. Figure 3.0212.

3.0213 Effect of silicon content on room temperature tensile properties. Figure 3.0213.

3.0214 Effect of time and temperature of exposure on room temperature tensile strength. Figure 3.0214.

3.0215 Effect of time and temperature of exposure on room temperature yield strength. Figure 3.0215.

3.0216 Effect of time and temperature of exposure on room temperature tensile elongation. Figure 3.0216.

3.0217 Tensile properties of as-cast specimens and specimens machined from turbine blades of standard and hafnium-modified alloy. Table 3.0217.

3.022 Compression.

3.0221 Stress-strain diagrams.

3.023 Impact.

3.0231 Relative impact strengths of alloy with several proprietary aluminum-base coatings. Figure 3.0231.

3.024 Bending.

3.025 Torsion and shear.

3.026 Bearing.

3.027 Stress concentration.

3.0271 Notch properties.

3.0272 Fracture toughness.

3.028 Combined properties.

3.03 **Mechanical Properties at Various Temperatures**

3.031 Tension.

3.0311 Stress-strain curves of as-cast alloy from 1200 to 2000 F. Figure 3.0311.

3.0312 Effect of test temperature on tensile properties of as-cast bar. Figure 3.0312.

3.0313 Tensile properties from 1200 to 2000 F for coated and heat treated bar used in thermal fatigue investigation cited in Figure 3.0533. Figure 3.0313.

3.0314 Effect of vacuum and argon casting on tensile properties at room and elevated temperatures. Figure 3.0314.

3.0315 Yield strength for alloy with 1.2 percent hafnium addition. Figure 3.0315.

3.0316 Effect of silicon content on 1200 F tensile properties. Figure 3.0316.

3.0317 Effect of time and temperature of exposure on ultimate tensile strength at 1400 F. Figure 3.0317.

3.0318 Effect of time and temperature of exposure on tensile yield strength at 1400 F. Figure 3.0318.

3.0319 Effect of time and temperature of exposure on tensile elongation at 1400 F. Figure 3.0319.

| | |
|---|---|
| 3.032 | Compression. |
| 3.0321 | Stress-strain diagrams. |
| 3.033 | Effect of melt atmosphere on Charpy V impact strength at room and elevated temperatures. Figure 3.033. |
| 3.034 | Bending. |
| 3.035 | Torsion and shear. |
| 3.036 | Bearing. |
| 3.037 | Stress concentration. |
| 3.0371 | Notch properties. |
| 3.0372 | Fracture toughness. |
| 3.038 | Combined properties. |
| 3.04 | **Creep and Creep-Rupture Properties** |
| 3.041 | Creep. |
| 3.0411 | Times to produce 1 percent creep at temperatures from 1500 to 2000 F for alloy in as-cast, heat treated, or coated and heat treated condition, Figure 3.0411. |
| 3.0412 | Typical stresses required to produce 1-percent creep in 100, 300, and 1000 hours for alloy in coated and heat treated condition, Figure 3.0412. |
| 3.0413 | Effect of exposure time and temperature on time to reach 1 percent elongation in a subsequent creep test at 1400 F, 94 ksi, Figure 3.0413. |
| 3.0414 | Effect of time and temperature of exposure on time to reach 1 percent creep in a subsequent creep test at 1800 F, 29 ksi, Figure 3.0414. |
| 3.0415 | Effect of hafnium addition on curves for 1 percent creep in 300 hours at temperatures from 1400 to 1800 F, Figure 3.0415. |
| 3.042 | Creep rupture. |
| 3.0421 | Creep rupture curves from 1500 to 2100 F for alloy in as-cast, heat treated, or coated and heat treated condition, Figure 3.0421. |
| 3.0422 | Typical stresses required to produce rupture in 100, 300, and 1000 hours for alloy in coated and heat treated condition, Figure 3.0422. |
| 3.0423 | Creep rupture curves at 1400 to 2000 F for conventionally cast and directionally solidified bar, Figure 3.0423. |
| 3.0424 | Shear rupture strength. The shear rupture strength is of interest to the design of dovetail root sections for fastening turbine blades to wheels. The shear rupture strength for B-1900 approximates 0.6 of the tensile rupture strength for 100-hour life (Figure 3.04241), similar to the ratios observed for other high strength alloys. |
| 3.04241 | Shear and tensile rupture strengths at 1400 F. Figure 3.04241. |
| 3.043 | Compositional effects on creep rupture. |
| 3.0431 | Effect of hafnium addition on 300 hour creep rupture curves, Figure 3.0431. |
| 3.0432 | Frequency analysis of B-1900 and B-1900-Hf creep rupture failures, Figure 3.0432. |
| 3.0433 | Creep rupture life and ductility of as-cast specimens and of specimens machined from cast turbine blades of standard and hafnium-modified alloy, Table 3.0433. |
| 3.0434 | Effect of silicon concentration on creep rupture life at 22 ksi, 1832 F. Figure 3.0434. |
| 3.0435 | Effect of various heat treatments and silicon content on rupture ductility at 1832 F, 22 ksi, Figure 3.0435. |
| 3.0436 | Effect of lead content on creep rupture life at 1800 F, 29 ksi, Figure 3.0436. |
| 3.044 | Prior exposure effects and protective systems. |
| 3.0441 | Effect of time and temperature of exposure on creep rupture life at 1400 F, 94 ksi, Figure 3.0441. |
| 3.0442 | Effect of time and temperature of exposure on creep rupture life in a subsequent creep rupture test at 1800 F, 29 ksi, Figure 3.0442. |
| 3.0443 | Effect of time and temperature of prior exposure on ductility in a subsequent creep rupture test at 1400 F, 94 ksi, Figure 3.0443. |
| 3.0444 | Effect of time and temperature of prior exposure on ductility in a subsequent creep rupture test at 1800 F, 29 ksi, Figure 3.0444. |
| 3.045 | Stress concentration effects. |
| 3.0451 | Effect of heat treatment on notched bar creep rupture life at 94 ksi, 1400 F for two grain sizes, Figure 3.0451. |
| 3.046 | Hot isostatic pressing. HIPing is used to reduce internal porosity from casting (Figure 1.0941) with subsequent improvements in rupture properties (Figures 3.0461 and 3.0462) and fatigue properties (Figure 3.0514). These improvements are most apparent in 1400 F properties. Thick sections do not show an improvement in 1800 F properties after HIPing, but thin sections show substantial improvement. Undesireable microstructural changes resulting from the HIP cycle can be alleviated by further heat treatment. HIPing is also useful in restoring properties of salvaged blades. |
| 3.0461 | Effect of HIPing on rupture life and elongation at 1400 F, 94 ksi, Figure 3.0461. |
| 3.0462 | Effects of HIPing and heat treatment on rupture life at 1800 F and 29 ksi of thin section (0.030 inch) alloy, Figure 3.0462. |
| 3.05 | **Fatigue Properties** |
| 3.051 | Properties of smooth sections. |
| 3.0511 | Strain controlled low cycle fatigue at 1300, 1700, and 2000 F, Figure 3.0511. |
| 3.0512 | Modified Goodman diagram for $10^7$ cycles at 1700 F, Figure 3.0512. |
| 3.0513 | Low cycle fatigue characteristics of smooth hollow specimen at 1300, 1700, and 2000 F in strain control cycling, Figure 3.0513. |
| 3.0514 | Effect of HIPing on fatigue life of smooth bar at 1400 F, Figure 3.0514. |
| 3.052 | Stress concentration effects. |
| 3.0521 | Low cycle fatigue characteristics at 1000 and 1700 F for tubular specimen with two sets of diagonal holes, Figure 3.0521. |
| 3.0522 | Low cycle fatigue characteristics at 1000 and 1700 F for tubular specimen with two sets of diagonal slots, Figure 3.0522. |
| 3.053 | Thermal shock and thermal fatigue. |
| 3.0531 | Thermal shock resistance of airfoil in as-cast and in coated and heat treated conditions, Figure 3.0531. |
| 3.0532 | Thermal fatigue crack resistance at maximum temperatures of 1800, 1900, and 2000 F for as-cast alloy samples subjected to high velocity oxidation cycling, Figure 3.0532. |
| 3.0533 | Thermal fatigue (crack initiation) in alternate fluidized beds at 600 and 1990 F of basic alloy, aluminide coated alloy, and alloy with hafnium additions, with comparison to other superalloys. Figure 3.0533. |
| 3.0534 | Effect of hafnium additions on thermal fatigue resistance in fluidized bed at 1800 F. Figure 3.0534. |

| |
|---|
| Ni |
| 10 Co |
| 8 Cr |
| 6 Mo |
| 6 Al |
| 4 Ta |
| 1 Ti |
| + C |
| + Zr |
| + B |

B-1900

Ni
10 Co
8 Cr
6 Mo
6 Al
4 Ta
1 Ti
+ C
+ Zr
+ B

B-1900

3.0535 Some comparative properties of basic alloy and alloy with 1.64 percent hafnium, Table 3.0535.
3.054 Crack growth.
3.0541 Crack propagation at 800 F for alloy with hafnium addition, Figure 3.0541.
3.0542 Crack propagation in thermomechanical cycling of alloy with hafnium addition (mechanically imposed strain out of phase with temperature cycling), Figure 3.0542.
3.0543 Crack propagation in thermomechanical cycling of alloy with hafnium addition (mechanically imposed strain in phase with temperature variation during half of cycle and out of phase in other half), Figure 3.0543.
3.0544 Crack propagation under thermomechanical cycling of alloy with hafnium addition (mechanically imposed strain in phase with temperature cycling), Figure 3.0544.
3.055 Protective systems.
3.0551 Effect of heating (and equal cooling) time on crack initiation in thermal fatigue of bare and coated specimens alternately immersed in hot and cold fluidized beds, Figure 3.0551.
3.0552 Low cycle fatigue at 1400 F of uncoated alloy and of alloy coated by a single heating cycle with an aluminized coating using Ni-15Cr-15Co-1Si as modifier, Figure 3.0552.
3.0553 Low cycle fatigue at 1400 F of uncoated alloy and of alloy coated by a duplex cycle with an aluminized coating using Ni-20Cr-15Co as modifier, Figure 3.0553.

3.06 **Elastic Properties**
3.061 Poisson's ratio. Values of -0.2176, -0.2118, and -0.3771 at room temperature are reported (42).
3.062 Modulus of elasticity.
3.0621 Dynamic modulus of elasticity, Figure 3.0621.
3.0622 Static modulus of elasticity, Figure 3.0622.
3.063 Modulus of rigidity.

## 4 FABRICATION

4.01 **Forming**
4.011 Alloy is usually cast to shape.
4.012 Properties of thin sections required for cooled airfoils are somewhat lower than full airfoil blade shapes (19).
4.013 Gating configuration is critical to ensure good casting reproducibility and minimize microshrinkage (2).
4.0131 Alloy with hafnium addition has greater shrinkage characteristics than conventional alloy. Special gating and pouring practice required for this alloy is not the same as for conventional alloy.

4.02 **Machining and Grinding**
Similar to cast Udimet 500 and cast Mar-M-200.
4.021 This alloy is difficult to machine as it has a machinability rating of 18 percent (as compared to above 100 percent for aluminum). It machines similar to Inco 713, IN-100 and SM 200 alloys. Rigid equipment and flood cooling with soluble oils or water base chemical coolants are required. Feeds and speeds are generally lower than values used for steel machining. Sharp, hard cutting tools are recommended.
4.022 For turning, boring, and milling, carbide tools are recommended. All tools should have positive rake angles.
4.023 For drilling, "cobalt" high speed drills are recommended, though high speed steel twist drills can be used if they cut and do not smear (cold work) material. Thus, drill sharpness, speeds, and feeds must be controlled.
4.024 For grinding, aluminum oxide wheels are generally used.

4.03 **Joining**
4.031 Welding. Repair welding in inert atmospheres using GTA process has been successfully applied. Either Hastelloy C or Hastelloy X filler at 1300 F preheat, or parent metal filler at 1750 F preheat can be employed (2).

4.04 **Surface Treating**

## REFERENCES


1 Piearcey, B. J. and Terkelson, B. E., "The Effect of Unidirectional Solidification on the Properties of Cast Nickel-Base Superalloys," Transactions AIME, Vol. 239 (August 1967), pp 1143-1150.
2 Pratt and Whitney Aircraft Communication to MPDC.
3 Donachie, M. J., Brody, R. P., and Bradley, E. F., "Thermal Fatigue of Turbine Alloys with Special Reference to PWA 663 Nickel-Base Alloy," SAE Preprint 66056, Automotive Engineering Congress, Detroit, Michigan (January 1966).
4 Inco, "High Temperature Strength of Nickel-Base Alloys" (1964).
5 Collins, H. E. and Quigg, R. J., "Carbide and Intermetallic Instability in Advanced Nickel-Base Alloys," ASM Transactions Quarterly, 61 (March 1968).
6 Stewart, O. L. and Vogel, W. H., "Methods for Predicting Thermal Stress Cracking in Turbine Stator or Rotor Blades," NASA CR-54636 (July 10, 1967).
7 Johnston, J. R. and Ashbrook, R. L., "Oxidation and Thermal Fatigue Cracking of Nickel and Cobalt-Base Alloys in High Velocity Gas Stream," NASA TN D-5376 (August 1969).
8 Spera, D. A., Calfo, F. D., and Bizon, P. T., "Thermal Fatigue Testing of Turbine Blades," NASA TMX-67820 (May 13, 1971).
9 Collins, H. E., "Research on Microstructural Instability of Nickel-Base Superalloys," AFML-TR-68-256 (October 1968).
10 Moore, V. S., Brentnall, W. D., and Stetson, A. R., "Evaluation of Coatings for Cobalt and Nickel Base Alloys," NASA CR-72714 (July 1970).
11 Spera, D. A., Howes, M.A.H., and Bizon, P. T., "Thermal Fatigue Resistance of 15 High Temperature Alloys Determined by the Fluidized-Bed Technique," NASA TM X-52975 (March 1971).
12 Leverant, G. R. and Dahl, D. N., "The Effect of Stress and Temperature on the Extent of Primary Creep in Directionally Solidified Nickel-Base Superalloys," Transactions AIME, Vol. 2 (March 1971), pp 907-908.

13 United Aircraft Research Laboratory, "Final Report of the Investigation of Sulfidation Mechanism in Nickel Base Superalloys," U.S. Naval Ship Research and Development Laboratory, Annapolis, Maryland, Contract No. N00600-68-C-0639 (April 1969).

14 Jackson, C. M. and Hall, A. M., "Surface Treatments for Nickel and Nickel-Base Alloys," NASA TM X-53448 (April 1966).

15 Schirmer, R. M. and Quigg, H. T., "Effect of Very Low Sulfur in JP-5 Fuel on Hot Corrosion," Proceedings of the Tenth National Conference on Environmental Effects on Aircraft and Propulsion Systems, Naval Air Propulsion Center, Trenton, New Jersey (May 1971).

16 Kaufman, A., Berry, T. F., and Meiners, K. E., "Joining Techniques for Fabrication of Composite Air-Cooled Turbine Blades and Vanes," NASA TMX-52877 (April 1971).

17 Pratt and Whitney Spec, PWA 663, Revision T (March 1971).

18 Pratt and Whitney Spec, PWA 1455, Revision D (March 1971).

19 Martin Metals Communication to MPDC (1971).

20 Inouye, S. and George, Saul, "Arc Melting Superalloys for Extrusion Studies," Technical Report No. AFML-TR-66-278 (November 1966).

21 Collins, H. E., "The Effect of Simulated Jet Engine Thermal Conditions on the Microstructure and Mechanical Properties of the Nickel-Base Superalloy B-1900," TRW TM-4591 (1971).

22 Moore, V. S. and Stetson, A. R., "Hot Corrosion Resistant Aluminide Coatings of Controlled Composition for Nickel-Base Superalloys," Naval Air Propulsion Center, Trenton, New Jersey (July 1973).

23 Sanders, W. A., "Dynamic Oxidation Behavior at 1000C and 1100C of Four Nickel-Base Cast Alloys, NASA-TRW VI A, B-1900, 713C and 738X," NASA TN D-7682 (August 1974).

24 Walters, J. J., "Study of the Hot Corrosion of Superalloys," AFML-TR-67-297 (September 1967).

25 Lowell, C. E. and Probst, H. B., "Effects of Composition and Testing Conditions on Oxidation Behavior of Four Cast Commercial Nickel-Base Alloys," NASA TN D-7705 (August 1974).

26 Dunn, R. G., Sponseller, D. L. and Dahl, J. M., "Ductility Improvements in Superalloys", Proceedings of Conference *Toward Improved Ductility and Toughness, Kyoto,* the Iron and Steel Institute of Japan and the Japan Institute of Metals (October 1971).

27 Hackin, J. and Taylor, W., Second World Conference on Investment Castings, Dusseldorf, Germany (June 1969).

28 Miner, R. V. and Lowell C. E., "Effects of Silicon Additions on the Oxidation and Mechanical Behavior of the Nickel-Base Superalloy B-1900," NASA TN-D-7989 (June 1975).

29 Leverant, G. R., Strangman, T. E., and Langer, B.S., "Parameters Controlling the Thermal Fatigue Properties of Conventionally-Cast and Directionally-Solidified Turbine Alloys," Proceedings of the Superalloys, Metallurgy and Manufacture 3rd International Symposium, Seven Springs, Pennsylvania (1976) pp 285-294.

30 Gemma, A. E., Langer, B. S., and Leverant, G. R., "Thermomechanical Fatigue Crack Propagation in an Anisotropic (Directionally-Solidified) Nickel-Base Superalloy," ASTM STP 612 (1976) pp 199-213.

31 Bizon, P. T. and Spera, D. A., "Comparative Thermal Fatigue Resistances of Twenty-six Nickel and Cobalt-Base Alloys," NASA TN D-8071 (October 1975).

32 Carnahan, D. R., Michlin, D. S., and DePierre, V., "Extrusion of Refractory Metals and Superalloys," AFML-TR-66-344 (December 1966).

33 Metals and Ceramics Information Center, "Trace Elements in Superalloys-Status Report," Vol. 4, No. 12 (December 1974).

34 Chandley, G. D., "Advances in Investment-Casting Technology," Proceedings of the First Army Materials Technical Conference on Solidification Technology, Wentworth-by-the-sea, Portsmouth, New Hampshire (1972) pp 189-208.

35 Nakagawa, Y. G., Ohtomo, A., and Saiga, Y., "Directional Solidification of Rene 80," Transactions, Japan Institute of Metals, Vol. 17 (1976) pp 323-329.

36 McLean, M. and Schubert, F., "Mechanical Properties of Directionally Solidified Superalloys and Eutectics," Proceedings of the Conference on High Temperature Alloys for Gas Turbines, Liege, Belgium (1978) pp 423-458.

37 Fryburg, G. C., Kohl, F. J., and Stearns, C. A., "Oxidation in Oxygen at 900 and 1000C of Four Nickel-Base Cast Superalloys: NASA-TRW VIA, B-1900, Alloy 713C, and IN-738," NASA TN D-8388 (January 1977).

38 Stearns, C. A., Kohl, F. J., and Fryburg, G. C., "Susceptibility to Hot Corrosion of Four Nickel-Base Superalloys, NASA-TRW VIA, B-1900, 713C, and IN-738," NASA TN D-8461 (April 1977).

39 Fryburg, G. C., Kohl, F. J., Stearns, C. A., and Fielder, W. L., "Chemical Reactions Involved in the Initiation of Hot Corrosion of B-1900 and NASA-TRW VIA," Journal of the Electrochemical Society, Vol. 129, No. 3 (March 1982) pp 571-585.

40 Glasgow, T. K., "Creep Shear Behavior of the Oxide Dispersion Strengthened Superalloy MA 6000E," NASA TM 82704, Prepared for 110th Annual Meeting of AIME, Chicago (February 22-26, 1981).

41 Freeman, W. R., Jr., "HIP'ing Raises Casting Performance Levels," Metal Progress, Vol. 112, No. 3 (August 1977) pp 33-38.

42 Fritz, L. J. and Koster, W. P., "Tensile and Creep Rupture Properties of (16) Uncoated and (2) Coated Engineering Alloys at Elevated Temperatures," NASA CR-135138 (January 15, 1977).

43 van der Vet, W. J., "HIP Processing—Potentials and Applications," Paper presented at 53rd Meeting of AGARD Structures and Materials, Panel, Maintenance in Service of High Temperature Parts, Noordwijkerhout, Netherlands (September 27-October 2, 1981) pp 11-1-11-16.


| Ni |
|---|
| 10 Co |
| 8 Cr |
| 6 Mo |
| 6 Al |
| 4 Ta |
| 1 Ti |
| + C |
| + Zr |
| + B |

B-1900

Ni
10 Co
8 Cr
6 Mo
6 Al
4 Ta
1 Ti
+ C
+ Zr
+ B

B-1900

| Alloy | PWA 663 | | PWA 1455 | |
|---|---|---|---|---|
| | Percent | | Percent | |
| Composition | Min | Max | Min | Max |
| Carbon | 0.08 | 0.13 | 0.08 | 0.13 |
| Manganese | – | 0.20 | – | 0.20 |
| Phosphorus | – | – | – | 0.015 |
| Sulfur | – | 0.015 | – | 0.015 |
| Silicon | – | 0.25 | – | 0.25 |
| Chromium | 7.50 | 8.50 | 7.50 | 8.50 |
| Cobalt | 9.50 | 10.50 | 9.50 | 10.50 |
| Molybdenum | 5.75 | 6.25 | 5.75 | 6.25 |
| Aluminum | 5.75 | 6.25 | 5.75 | 6.25 |
| Tantalum | 4.00 | 4.50 | 4.00 | 4.50 |
| Hafnium | – | – | 1.10 | 1.60 |
| Titanium | 0.80 | 1.20 | 0.80 | 1.20 |
| Boron | 0.010 | 0.020 | 0.010 | 0.020 |
| Zirconium | 0.05 | 0.10 | – | 0.13 |
| Iron | – | 0.35 | – | 0.35 |
| Tungsten | – | 0.10 | – | 0.10 |
| Columbium | – | 0.10 | – | 0.10 |
| Bismuth | – | 0.00005 | – | 0.00005 |
| Lead | – | 0.0010 | – | 0.0010 |
| Nickel | Balance | | Balance | |

TABLE 1.04. COMPOSITION

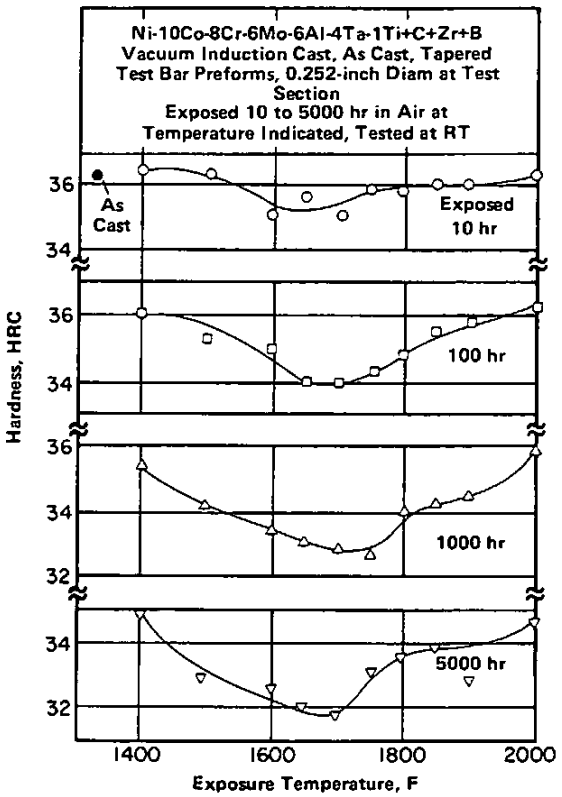


FIGURE 1.062. EFFECT OF TIME AND TEMPERATURE OF EXPOSURE ON ROOM TEMPERATURE HARDNESS (21)

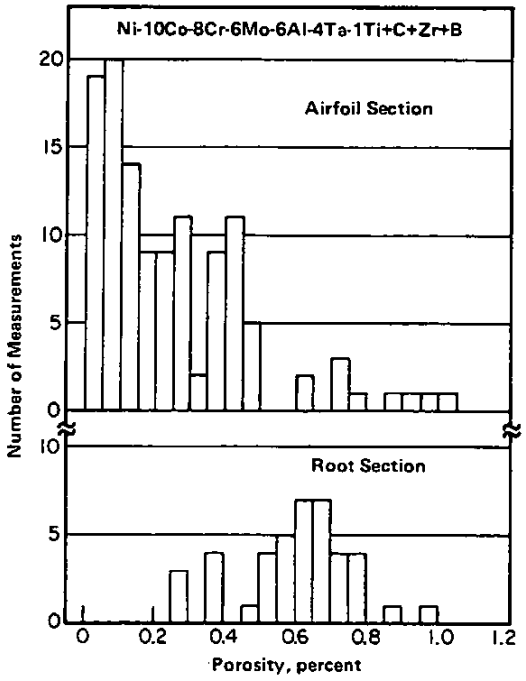


FIGURE 1.0941. NUMBER OF MEASUREMENTS AT VARIOUS POROSITY PERCENTAGES FOR CAST TURBINE BLADE AIRFOIL AND ROOT SECTIONS (34)

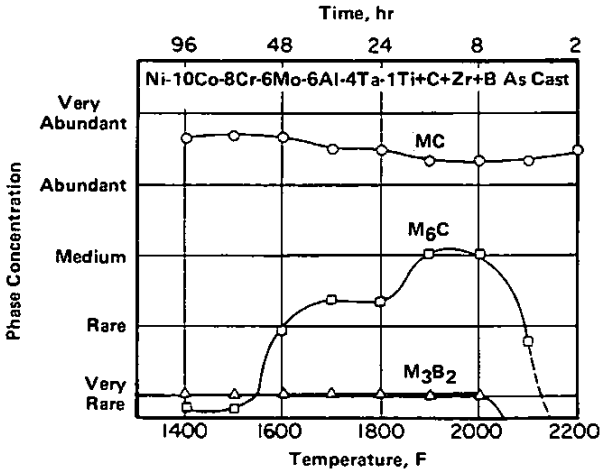


FIGURE 2.0121. MINOR PHASE CONCENTRATION FOR ALLOY AT VARIOUS TIMES AND TEMPERATURES (5,9)

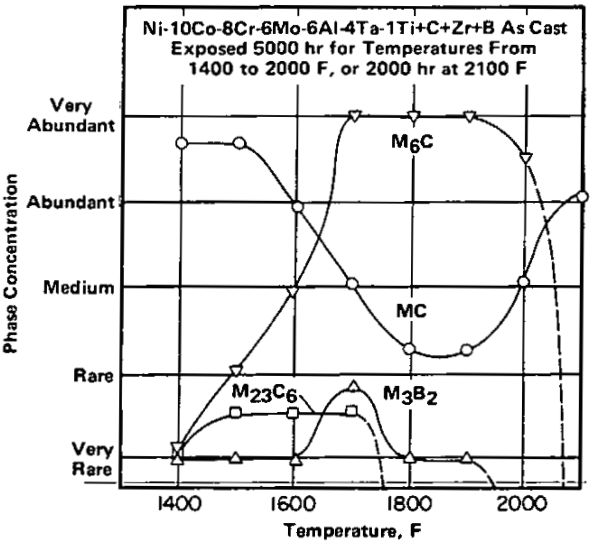


FIGURE 2.0122. MINOR PHASE CONCENTRATION FOR ALLOY AT LONG EXPOSURE TIMES FROM 1400 TO 2100 F (9)

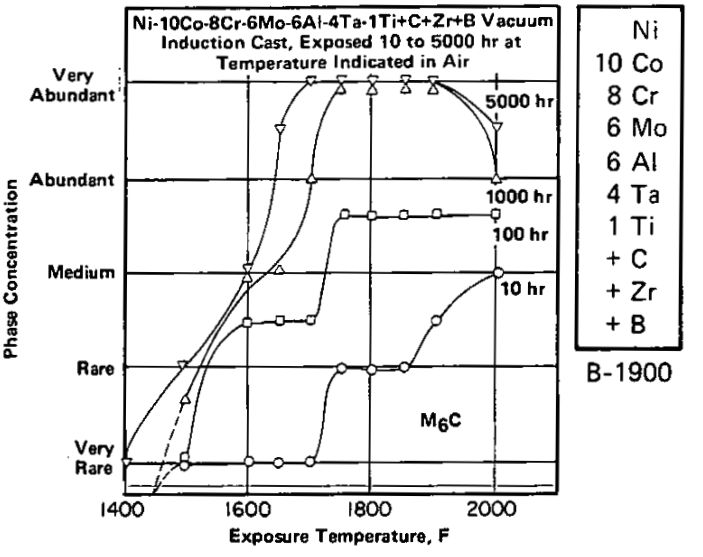


FIGURE 2.0123. EFFECT OF EXPOSURE TIME AND TEMPERATURE ON THE $M_6C$ PHASE (21)

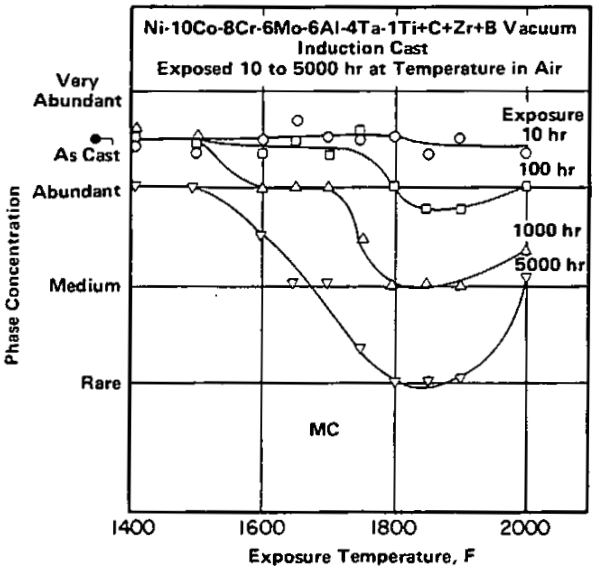


FIGURE 2.0124. EFFECT OF EXPOSURE TIME AND TEMPERATURE ON THE MC PHASE (21)

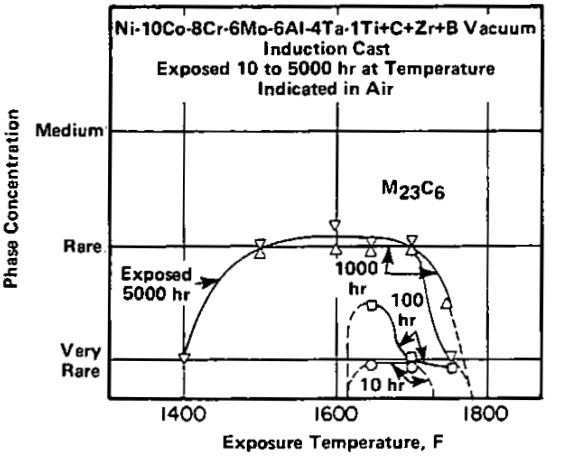


FIGURE 2.0125. EFFECT OF EXPOSURE TIME AND TEMPERATURE ON THE $M_{23}C_6$ PHASE (21)

Ni
10 Co
8 Cr
6 Mo
6 Al
4 Ta
1 Ti
+ C
+ Zr
+ B

B-1900

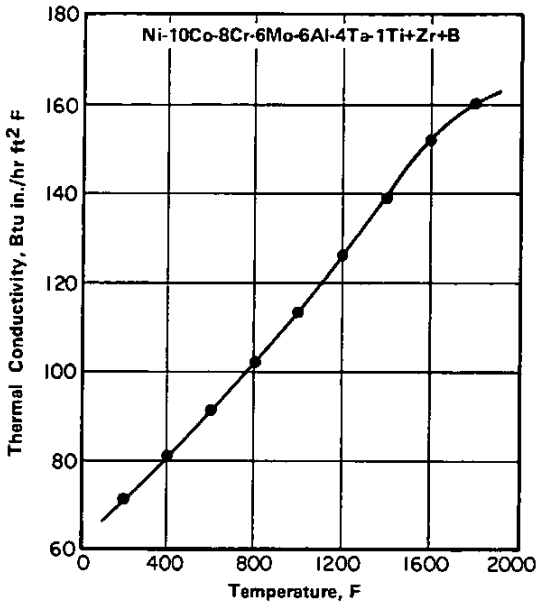


FIGURE 2.013. THERMAL CONDUCTIVITY (4)

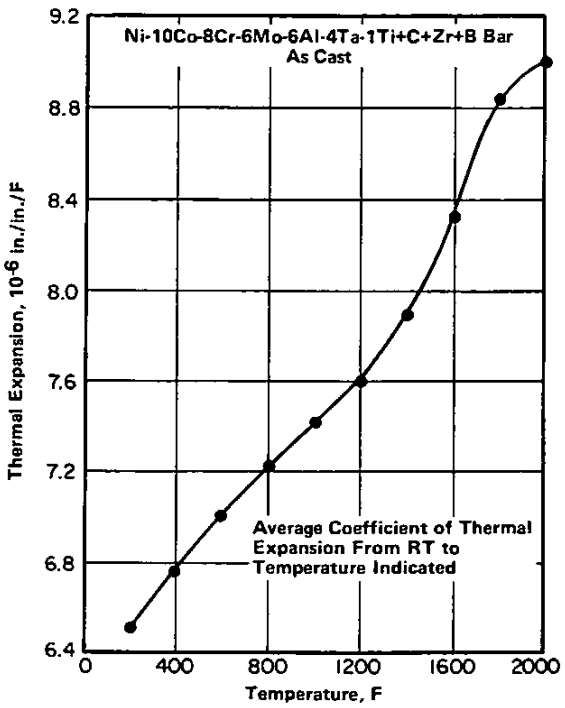


FIGURE 2.014. THERMAL EXPANSION (4)

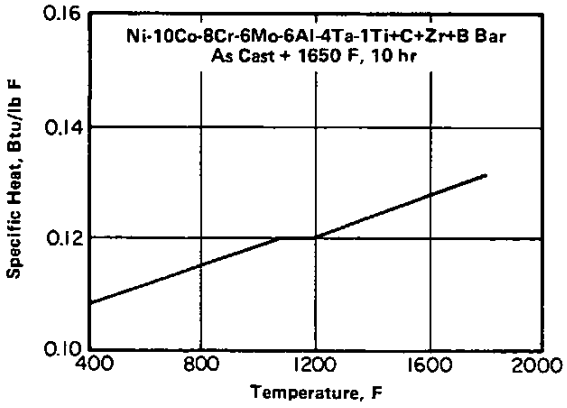


FIGURE 2.015. SPECIFIC HEAT (2,6)

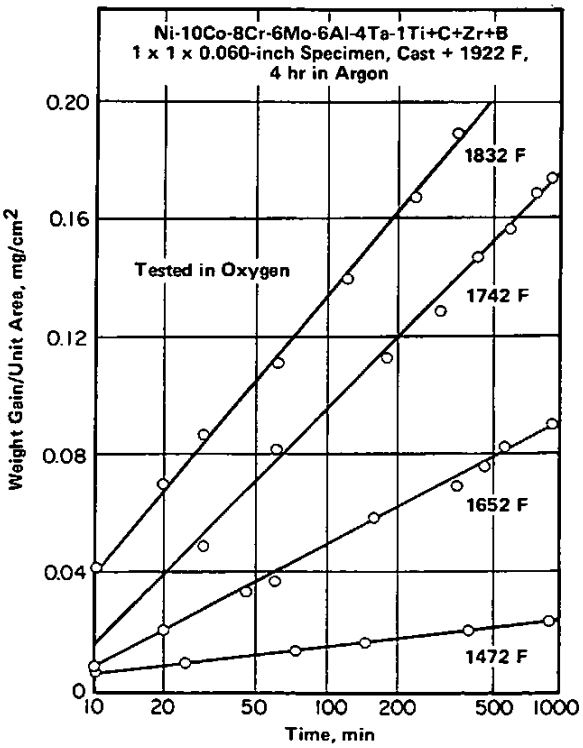


FIGURE 2.0311. OXIDATION KINETICS OF ALLOY (13)

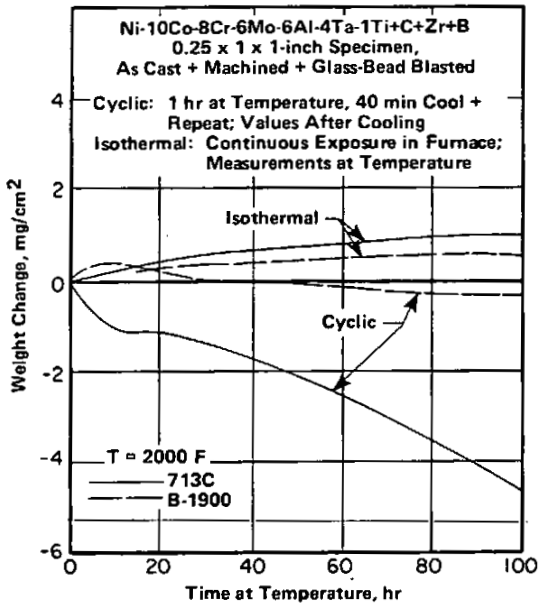


FIGURE 2.0312. STATIC AIR OXIDATION UNDER ISOTHERMAL AND CYCLIC CONDITIONS AT 2000 F WITH COMPARISON TO INCONEL 713C, ANOTHER NICKEL-BASE ALLOY (25)

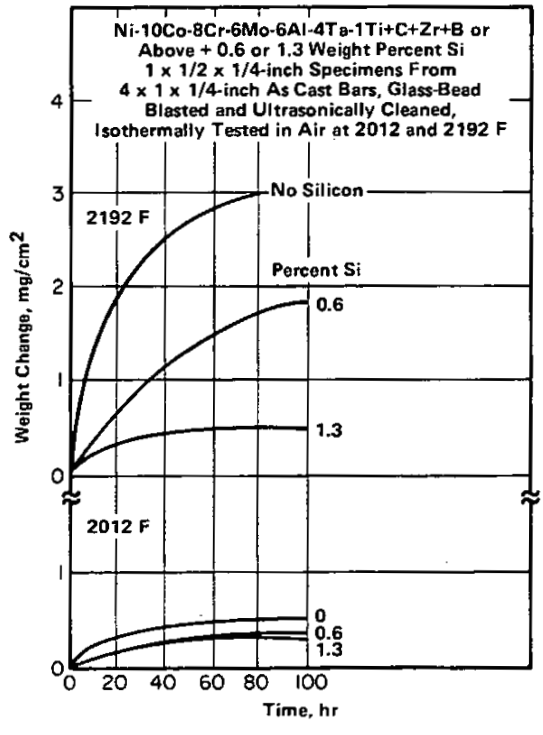


FIGURE 2.0314. EFFECT OF SILICON CONCENTRATION ON ISOTHERMAL OXIDATION AT 2012 AND 2192 F (28)

| Ni |
|---|
| 10 Co |
| 8 Cr |
| 6 Mo |
| 6 Al |
| 4 Ta |
| 1 Ti |
| + C |
| + Zr |
| + B |

B-1900

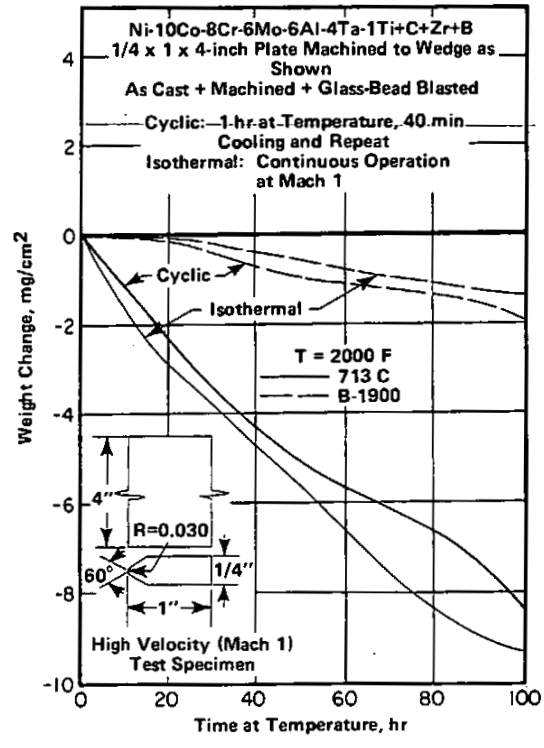


FIGURE 2.0313. HIGH VELOCITY (MACH 1) OXIDATION UNDER ISOTHERMAL AND CYCLIC CONDITIONS AT 2000 F WITH COMPARISON TO INCONEL 713C, ANOTHER NICKEL-BASE ALLOY (25)

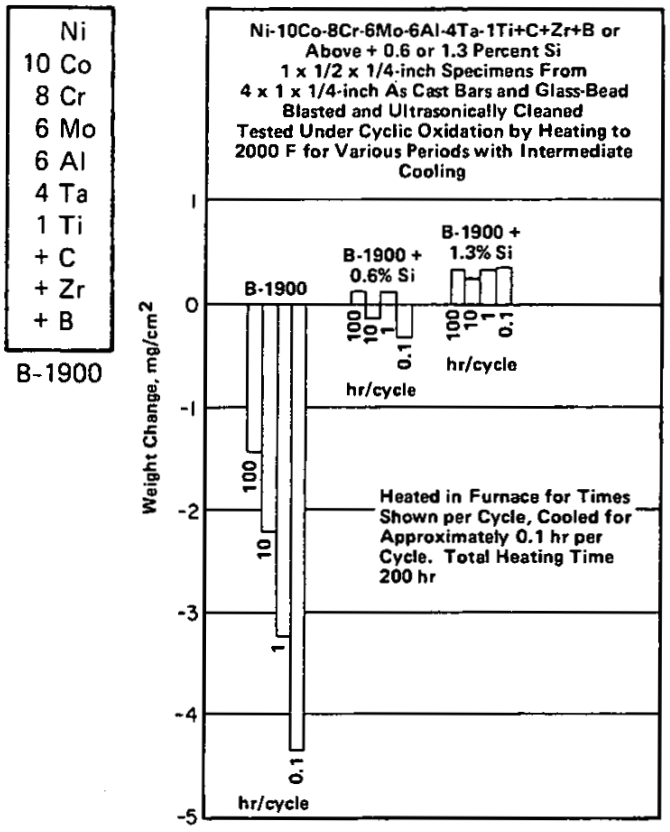


FIGURE 2.0315. EFFECT OF CYCLE PERIOD AND SILICON CONCENTRATION ON CYCLIC FURNACE OXIDATION (28)

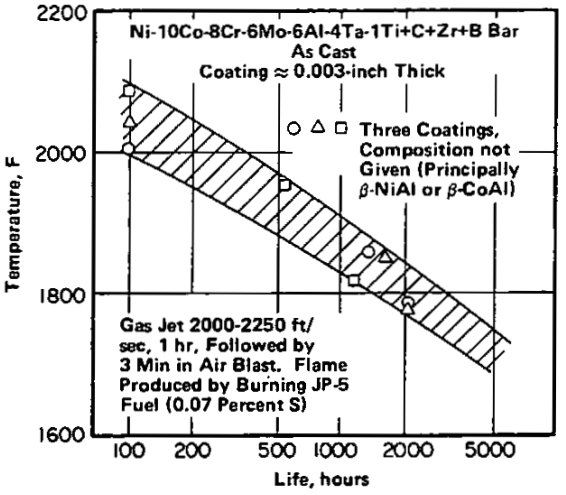


FIGURE 2.0316. EFFECT OF TEMPERATURE ON LIFE OF COATING SUBJECTED TO HIGH VELOCITY (MACH 0.8) COMBUSTION JET (10)

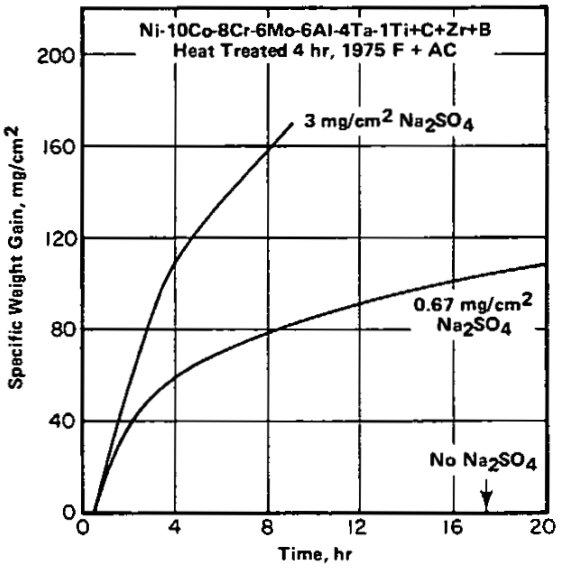


FIGURE 2.0321. EFFECT OF PRECOATING WITH $Na_2SO_4$ ON HOT CORROSION WEIGHT GAIN IN SLOWLY FLOWING OXYGEN AT 1832 F (38)

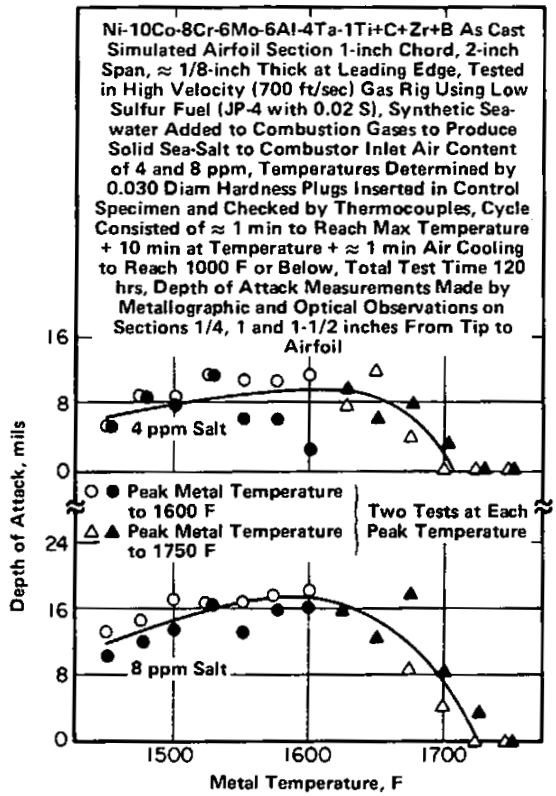


FIGURE 2.0322. CORROSION (AS MEASURED BY DEPTH OF ATTACK) FOR ALLOY IN 700 FPS VELOCITY GAS JET USING LOW SULFUR FUEL (JP-4) WITH 4 PPM AND 8 PPM SEA SALT IN INLET AIR (24)

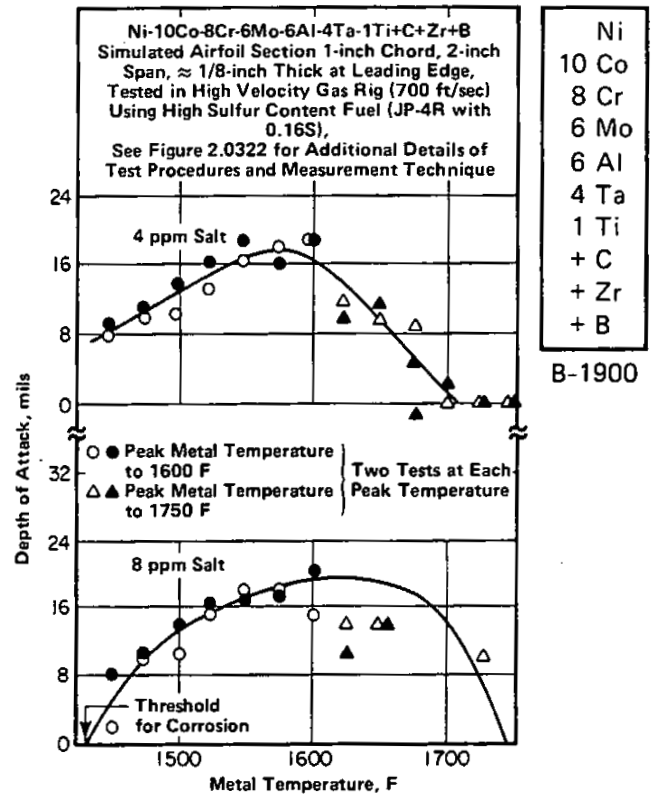


FIGURE 2.0323. CORROSION (AS MEASURED BY DEPTH OF ATTACK) FOR ALLOY IN 700 FPS VELOCITY GAS JET USING HIGH SULFUR FUEL (JP-4R) WITH 4 PPM AND 8 PPM SEA SALT IN INLET AIR (24)

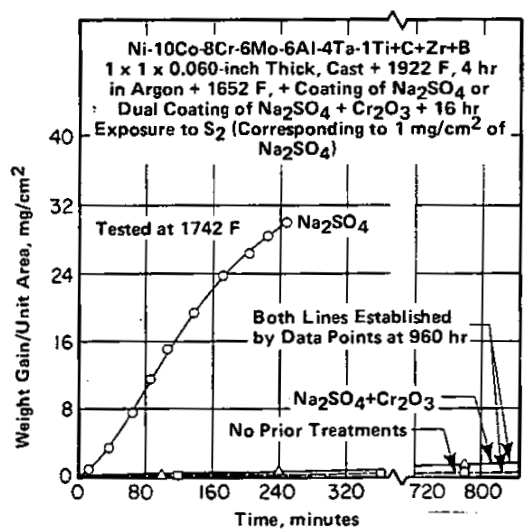


FIGURE 2.0324. EFFECT OF CHROMIA ADDITIVES ON SULFIDATION OF ALLOY AT 1742 F (13)

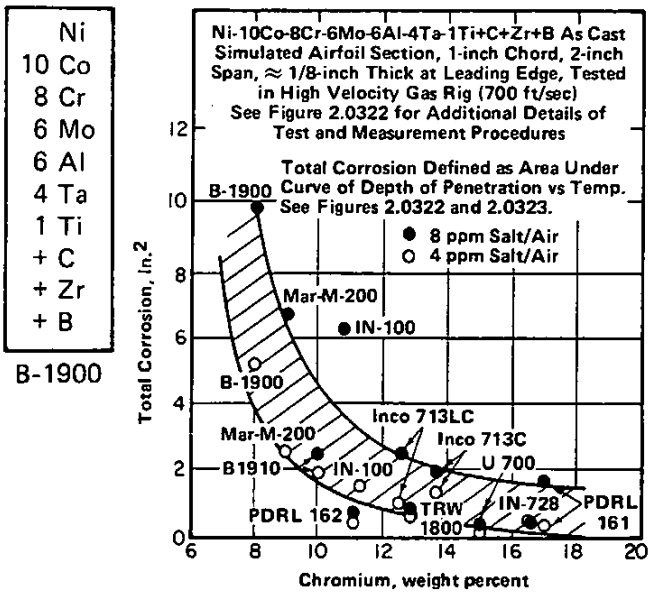


FIGURE 2.0325. CORRELATION SHOWING THAT LOW CORROSION RESISTANCE OF ALLOY IS RELATED TO ITS LOW CHROMIUM CONTENT (24)

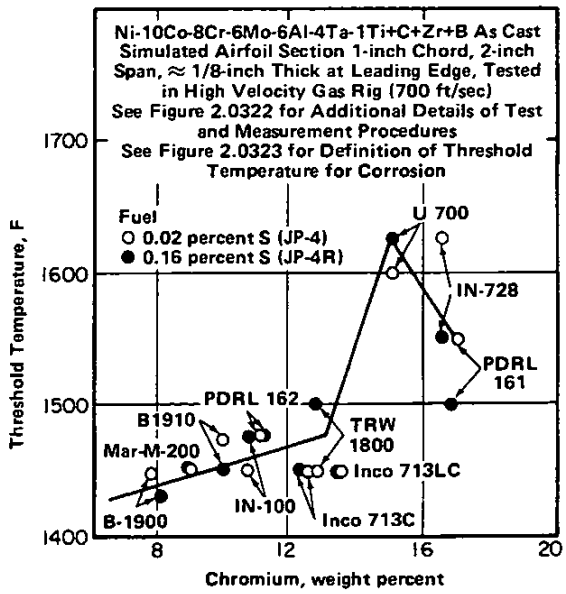


FIGURE 2.0326. CORRELATION SHOWING THAT THE LOW THRESHOLD TEMPERATURE FOR CORROSION IS PRINCIPALLY RELATED TO ITS LOW CHROMIUM CONTENT (24)

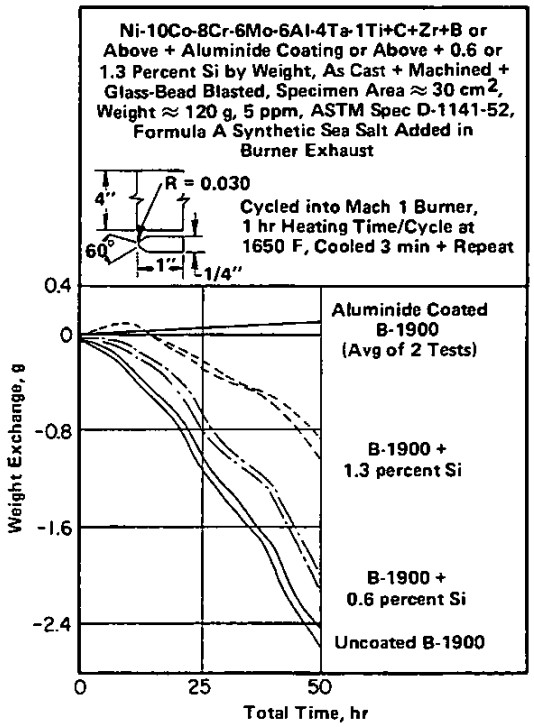


FIGURE 2.0327. EFFECT OF SILICON CONCENTRATION ON RESISTANCE TO HOT CORROSION IN MACH 1 BURNER EXHAUST AND COMPARISON WITH ALUMINIDE-COATED SPECIMEN (28)

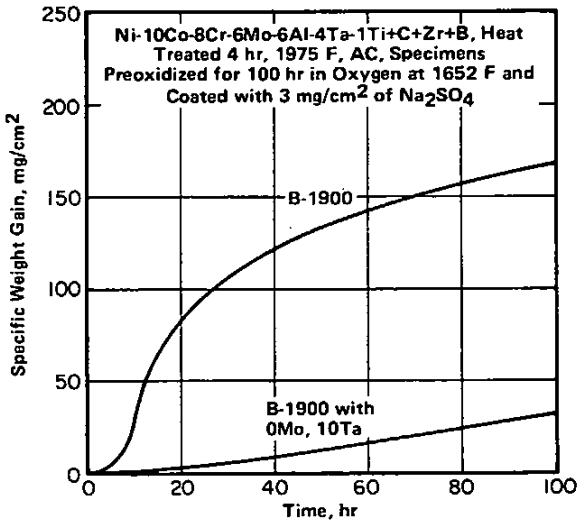


FIGURE 2.0328. EFFECT OF SUBSTITUTING TANTALUM FOR MOLYBDENUM ON HOT CORROSION BEHAVIOR AT 1652 F IN SLOWLY FLOWING OXYGEN (39)

| Alloy | | PWA 663 | PWA 1455 |
|---|---|---|---|
| Heat Treatment | Cast + 1975F, 4 hr, AC + 1650F, 10 hr, AC | | |
| Room Temperature Tensile Properties | | | |
| Ultimate Tensile Strength ($F_{tu}$), ksi (Min) | | – | 120 |
| Yield Strength ($F_{ty}$), ksi (Min) | | – | 105 |
| Elongation (4D), percent (Min) | | – | 5 |
| Creep Rupture Tests of Cast Specimens | | | |
| Tested at 1400 F, 94 ksi | | | |
| Life, hours (Min) | | 23 | 23 |
| Plastic Extension (4D), percent (Min) | | 2 | 3 |
| Tested at 1800 F, 29 ksi | | | |
| Life, hours (Min) | | 30 | 30 |
| Elongation (4D Measured at RT After Rupture), percent (Min) | | 3 | 5.5 |
| Creep Rupture Tests of Specimens Machined From Blades | | | |
| Tested at 1400 F, 85 ksi | | | |
| Life, hours (Min) | | 23 | – |
| Plastic Extension (4D), percent (Min) | | 1.5 | – |
| Tested at 1400 F, 94 ksi | | | |
| Life, hours (Min) | | – | 30 |
| Plastic Extension (4D), percent (Min) | | – | 2.5 |
| Tested at 1800 F, 29 ksi | | | |
| Life, hours (Min) | | – | 30 |
| Elongation (4D Measured at RT After Rupture), percent (Min) | | – | 4 |

TABLE 3.01. SPECIFIED MECHANICAL PROPERTIES (17,18)

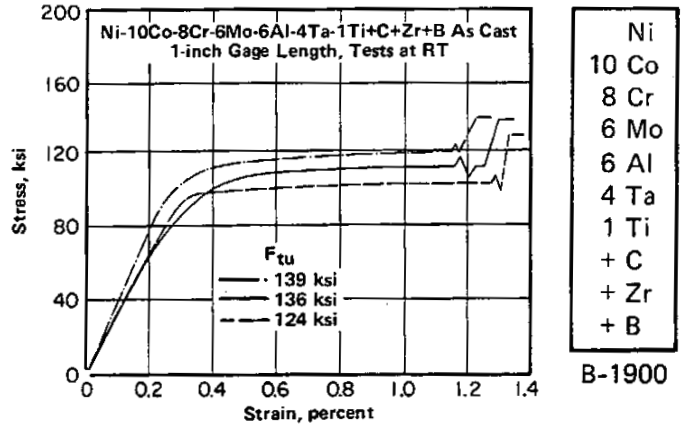


FIGURE 3.0211. STRESS-STRAIN CURVES FOR AS-CAST ALLOY (2)

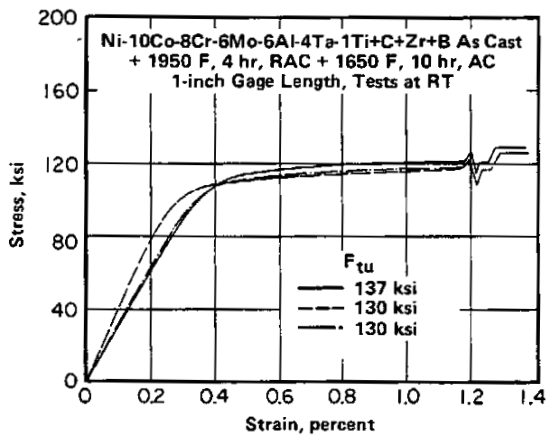


FIGURE 3.0212. STRESS-STRAIN CURVES FOR HEAT TREATED ALLOY (2)

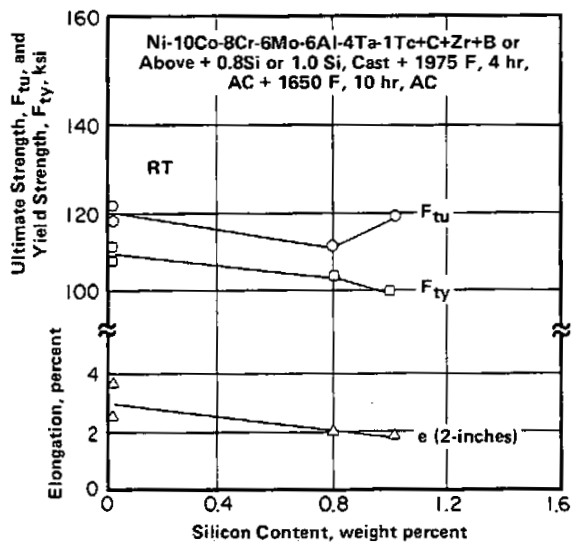


FIGURE 3.0213. EFFECT OF SILICON CONTENT ON ROOM TEMPERATURE TENSILE PROPERTIES (28)

Ni
10 Co
8 Cr
6 Mo
6 Al
4 Ta
1 Ti
+ C
+ Zr
+ B

B-1900

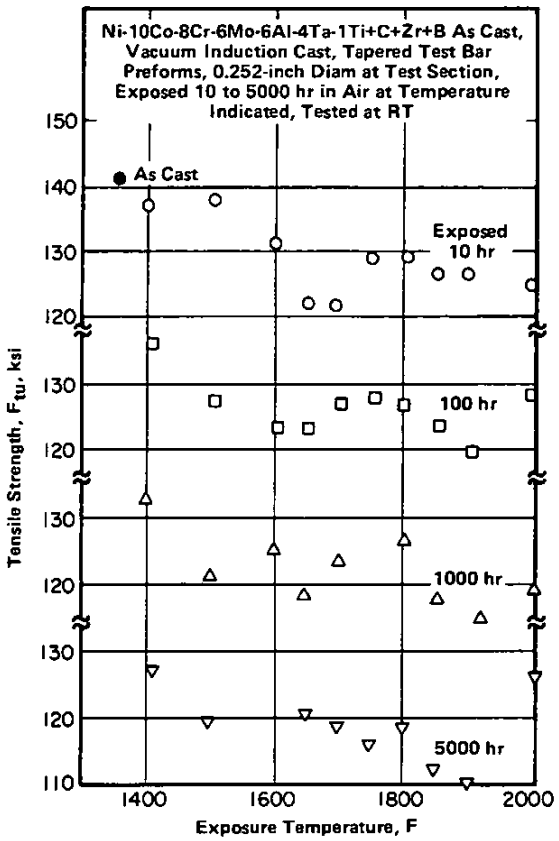


FIGURE 3.0214. EFFECT OF TIME AND TEMPERATURE OF EXPOSURE ON ROOM TEMPERATURE TENSILE STRENGTH (21)

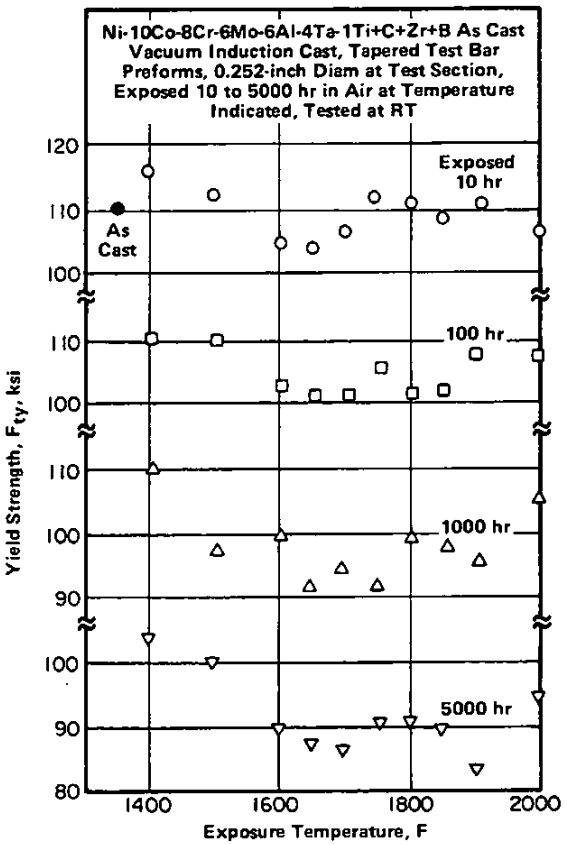


FIGURE 3.0215. EFFECT OF TIME AND TEMPERATURE OF EXPOSURE ON ROOM TEMPERATURE YIELD STRENGTH (21)

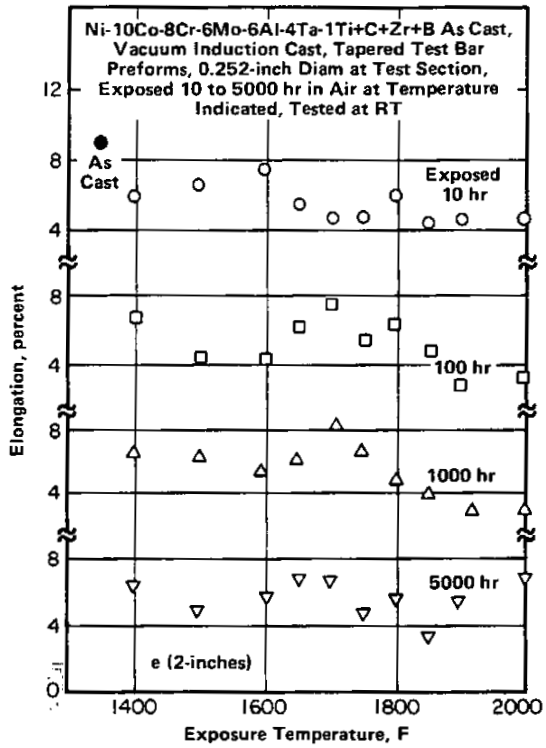


FIGURE 3.0216. EFFECT OF TIME AND TEMPERATURE OF EXPOSURE ON ROOM TEMPERATURE TENSILE ELONGATION (21)

| Alloy | Ni-10Co-8Cr-6Mo-6Al-4Ta-1Ti+C+Zr+B or Ni-10Co-8Cr-6Mo-6Al-4Ta-1.37Hf-1Ti-+C+Zr+B | | |
|---|---|---|---|
| Condition | As Cast | | |
| | B-1900 | | B-1900-Hf |
| Form | 1/4 Diam Cast to Size | 0.177 Diam From Cast Turbine Blades | 0.177 Diam From Cast Turbine Blades |
| RT | | | |
| $F_{tu}$, ksi | 135 | 115 | 127 |
| $F_{ty}$, ksi | 108 | 105 | 108 |
| e (2 inches), percent | 7.0 | 5.5 | 8.9 |

TABLE 3.0217. TENSILE PROPERTIES OF AS-CAST SPECIMENS AND SPECIMENS MACHINED FROM TURBINE BLADES OF STANDARD AND HAFNIUM-MODIFIED ALLOY (26,27)

| Ni |
|---|
| 10 Co |
| 8 Cr |
| 6 Mo |
| 6 Al |
| 4 Ta |
| 1 Ti |
| + C |
| + Zr |
| + B |

B-1900

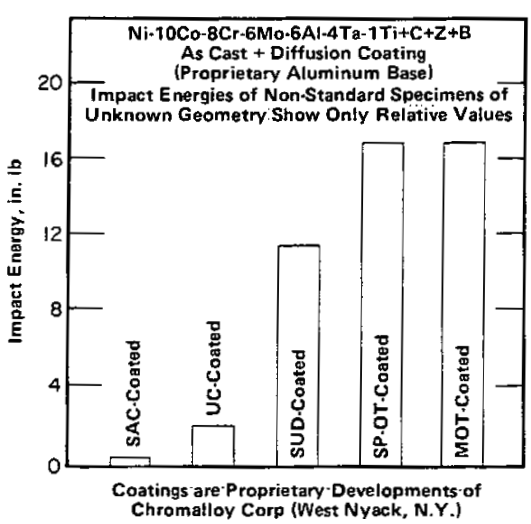


FIGURE 3.0231. RELATIVE IMPACT STRENGTHS OF ALLOY WITH SEVERAL PROPRIETARY ALUMINUM-BASE COATINGS (14)

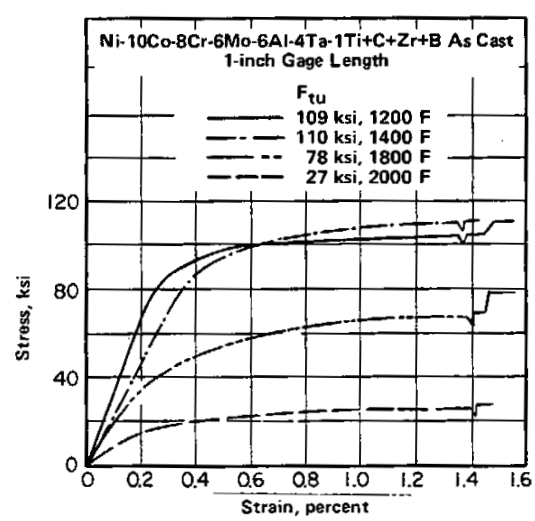


FIGURE 3.0311. STRESS-STRAIN CURVES FOR AS-CAST ALLOY FROM 1200 TO 2000 F

Ni
10 Co
8 Cr
6 Mo
6 Al
4 Ta
1 Ti
+ C
+ Zr
+ B

B-1900

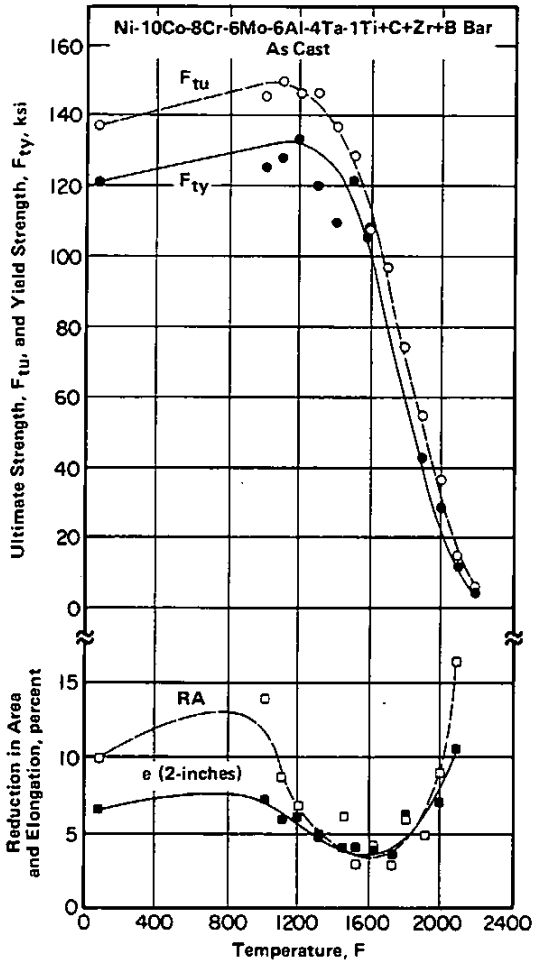


FIGURE 3.0312. EFFECT OF TEST TEMPERATURE ON TENSILE PROPERTIES OF AS-CAST BAR (2)

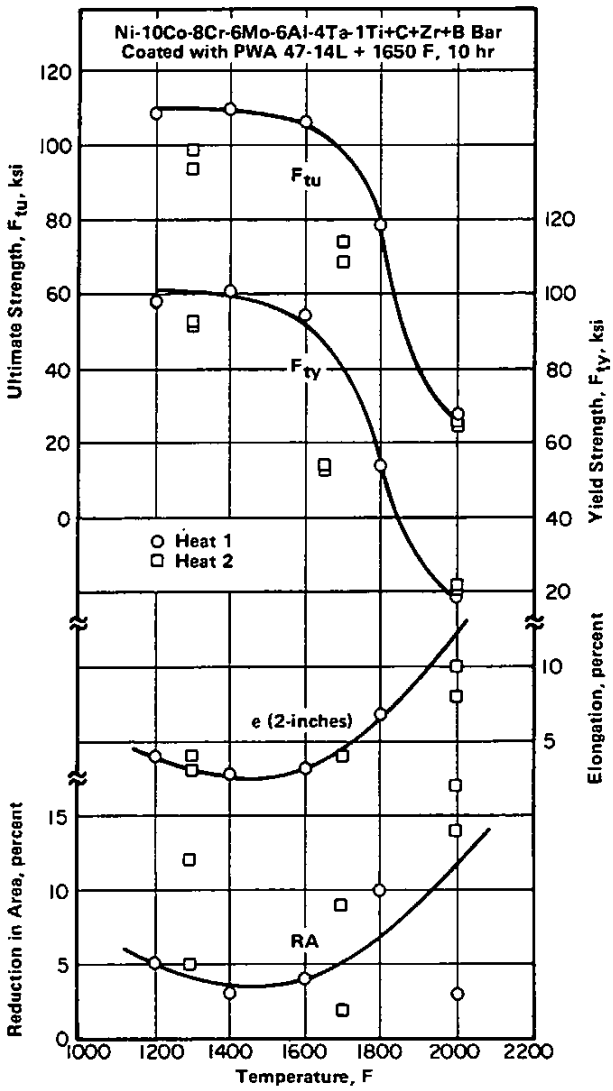


FIGURE 3.0313. TENSILE PROPERTIES FROM 1200 TO 2000 F FOR COATED AND HEAT TREATED BAR USED IN THERMAL FATIGUE INVESTIGATION CITED IN FIGURE 3.0533 (6)

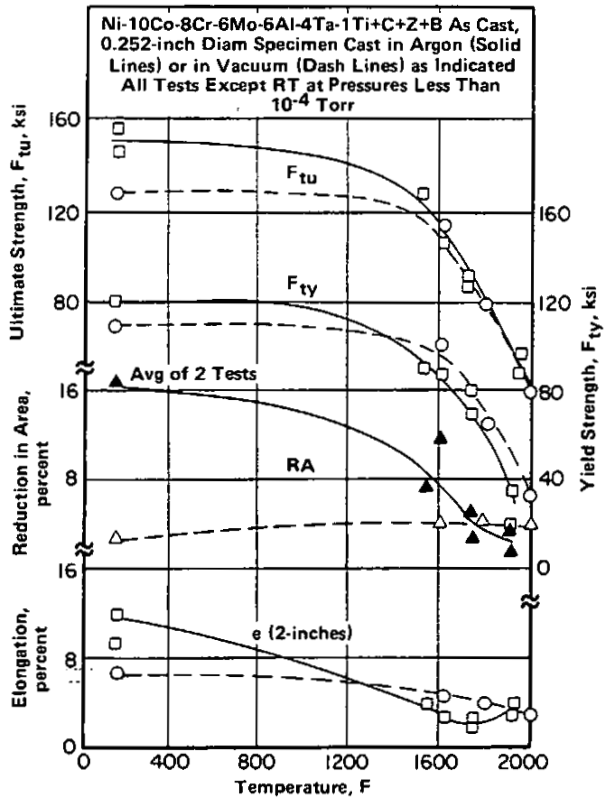


FIGURE 3.0314. EFFECT OF VACUUM AND ARGON CASTING ON TENSILE PROPERTIES AT ROOM AND ELEVATED TEMPERATURES (32)

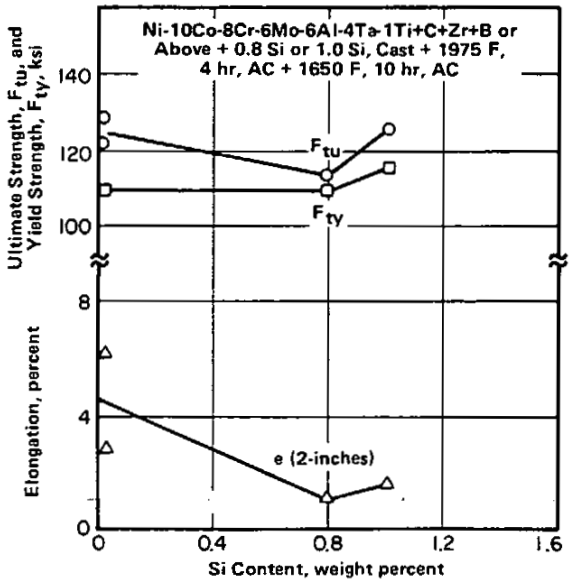


FIGURE 3.0316. EFFECT OF SILICON CONTENT ON 1200 F TENSILE PROPERTIES (28)

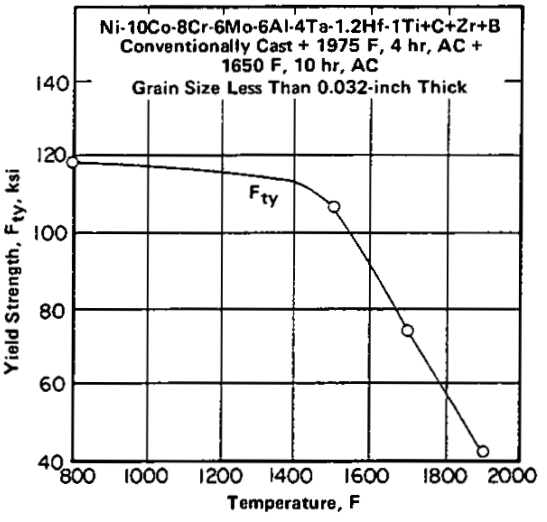


| Ni |
|---|
| 10 Co |
| 8 Cr |
| 6 Mo |
| 6 Al |
| 4 Ta |
| 1 Ti |
| + C |
| + Zr |
| + B |

B-1900

FIGURE 3.0315. YIELD STRENGTH FOR ALLOY WITH 1.2 PERCENT HAFNIUM ADDITION (30)

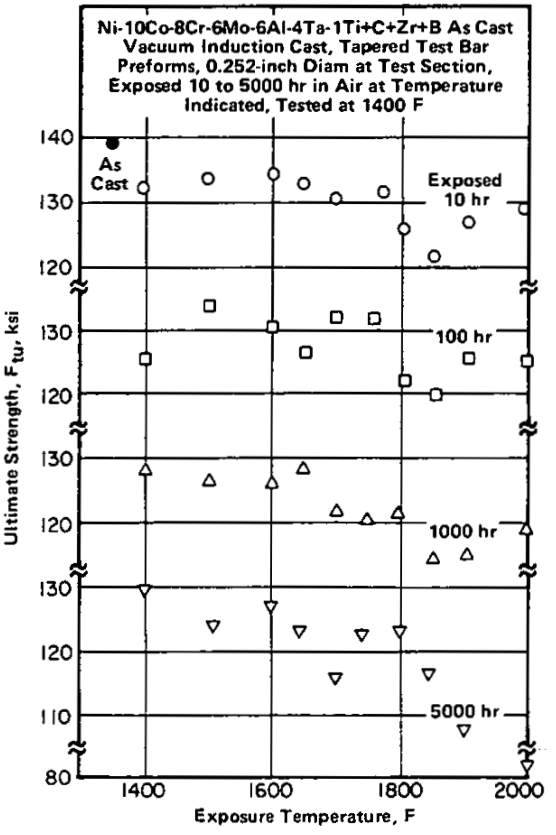


FIGURE 3.0317. EFFECT OF TIME AND TEMPERATURE OF EXPOSURE ON ULTIMATE TENSILE STRENGTH AT 1400 F (21)

Ni
10 Co
8 Cr
6 Mo
6 Al
4 Ta
1 Ti
+ C
+ Zr
+ B

B-1900

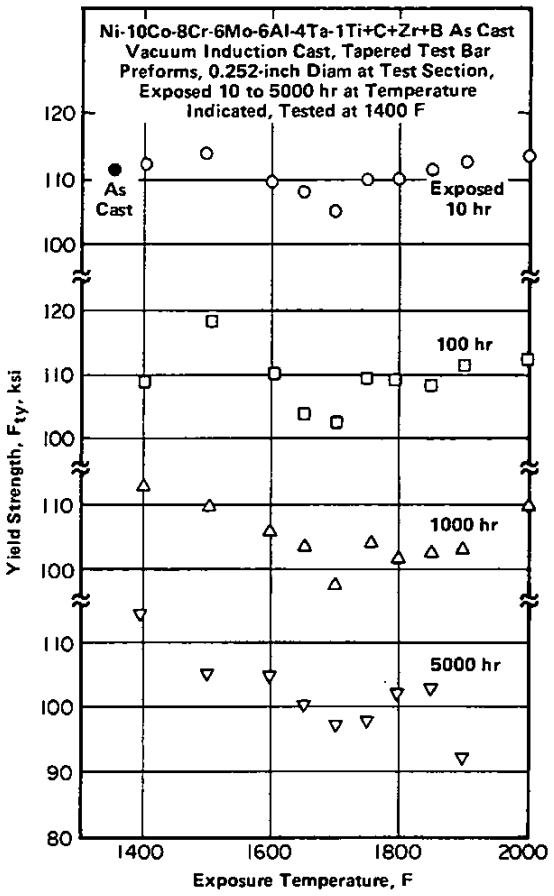


FIGURE 3.0318. EFFECT OF TIME AND TEMPERATURE OF EXPOSURE ON TENSILE YIELD STRENGTH AT 1400 F (21)

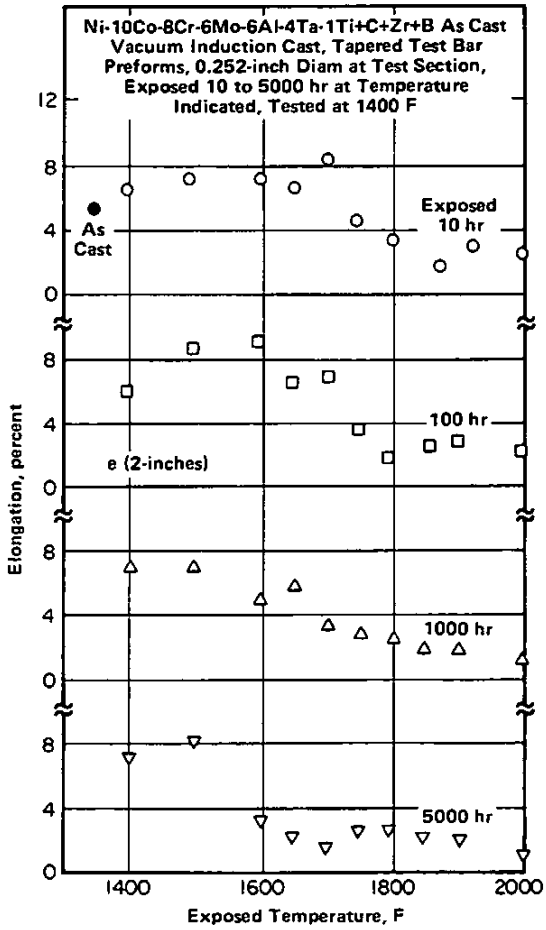


FIGURE 3.0319. EFFECT OF TIME AND TEMPERATURE ~~OF EXPOSURE ON TENSILE ELONGA-~~ TION AT 1400 F (21)

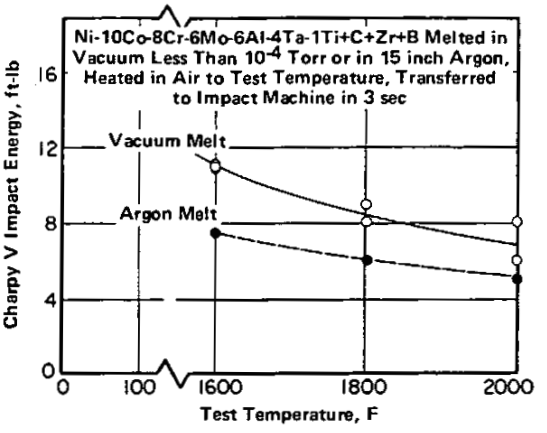


FIGURE 3.033. EFFECT OF MELT ATMOSPHERE ON CHARPY V IMPACT STRENGTH AT ROOM AND ELEVATED TEMPERATURES (20)

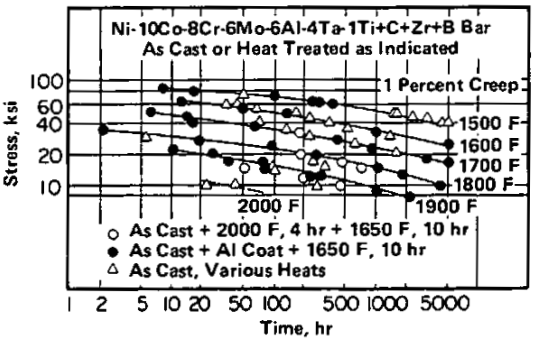


B-1900

FIGURE 3.0411. TIMES TO PRODUCE 1 PERCENT CREEP AT TEMPERATURES FROM 1500 TO 2000 F FOR ALLOY IN AS-CAST, HEAT TREATED, OR COATED AND HEAT TREATED CONDITION (2)

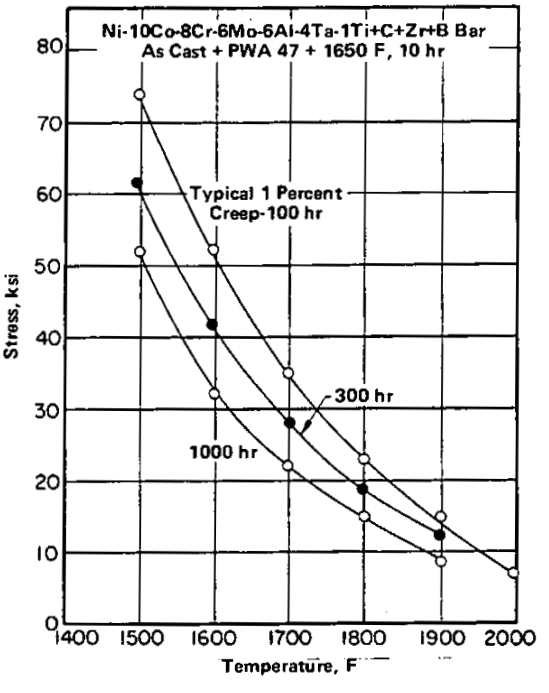


FIGURE 3.0412. TYPICAL STRESSES REQUIRED TO PRODUCE 1 PERCENT CREEP IN 100, 300, AND 1000 HOURS FOR ALLOY IN COATED AND HEAT TREATED CONDITION (2)

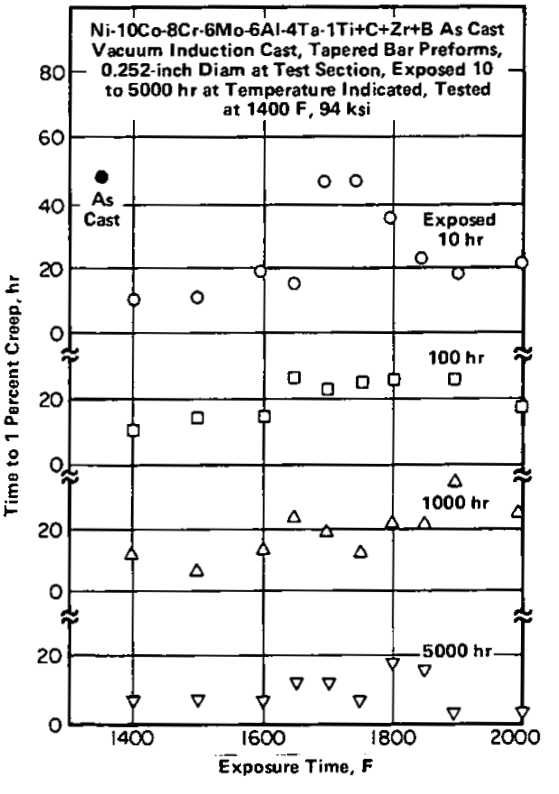


FIGURE 3.0413. EFFECT OF EXPOSURE TIME AND TEMPERATURE ON TIME TO REACH 1 PERCENT ELONGATION IN A SUBSEQUENT CREEP TEST AT 1400 F, 94 KSI (21)

Ni
10 Co
8 Cr
6 Mo
6 Al
4 Ta
1 Ti
+ C
+ Zr
+ B

B-1900

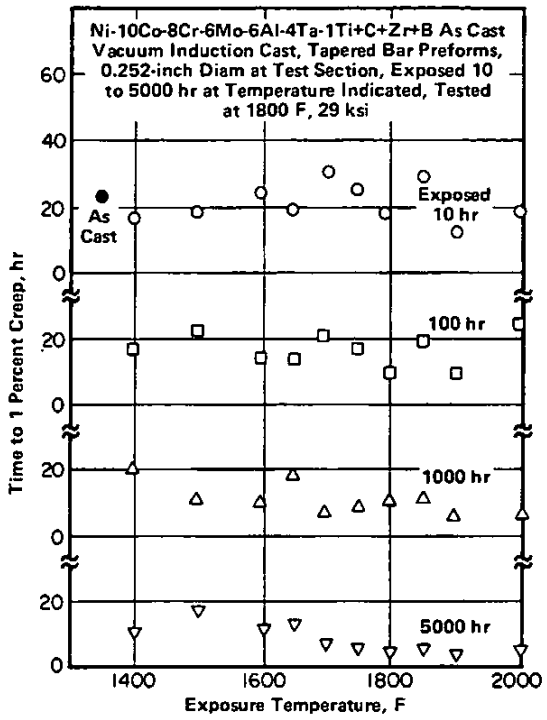


FIGURE 3.0414. EFFECT OF TIME AND TEMPERATURE OF EXPOSURE ON TIME TO REACH 1 PERCENT CREEP IN A SUBSEQUENT CREEP TEST AT 1800 F, 29 KSI (21)

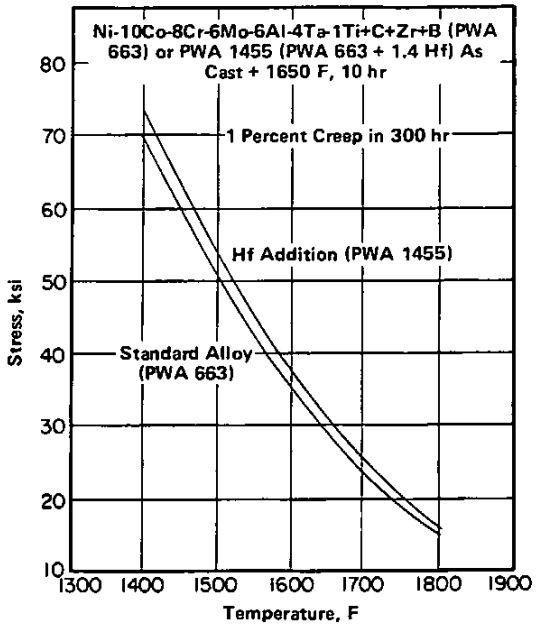


FIGURE 3.0415. EFFECT OF HAFNIUM ADDITION ON CURVES FOR 1 PERCENT CREEP IN 300 HOURS AT TEMPERATURES FROM 1400 TO 1800 F (2)

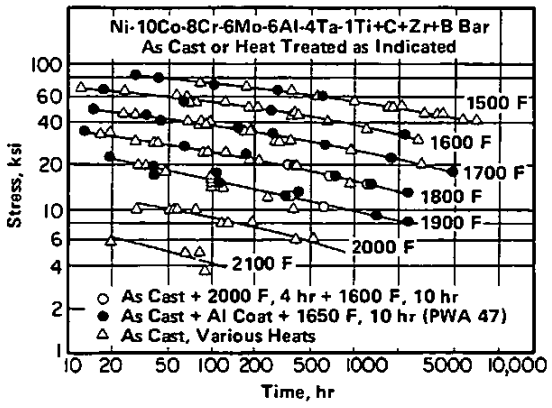


FIGURE 3.0421. CREEP RUPTURE CURVES FROM 1500 TO 2100 F FOR ALLOY IN AS-CAST, HEAT TREATED, OR COATED AND HEAT TREATED CONDITION (2)

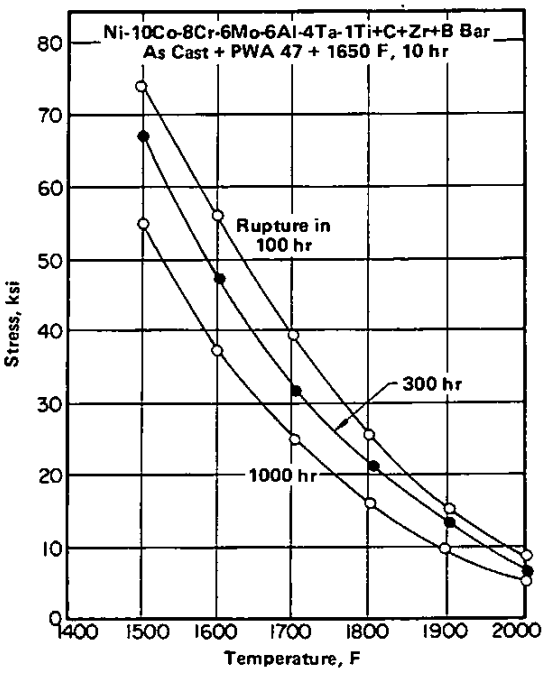


FIGURE 3.0422. TYPICAL STRESSES REQUIRED TO PRODUCE RUPTURE IN 100, 300, AND 1000 HOURS FOR ALLOY IN COATED AND HEAT TREATED CONDITION (2)

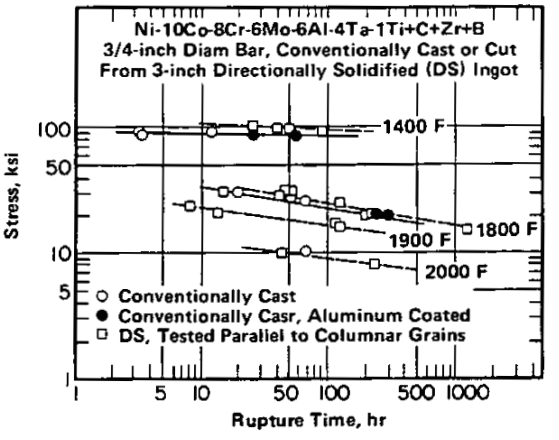


FIGURE 3.0423. CREEP RUPTURE CURVES AT 1400 TO 2000 F FOR CONVENTIONALLY CAST AND DIRECTIONALLY SOLIDIFIED BAR (1)

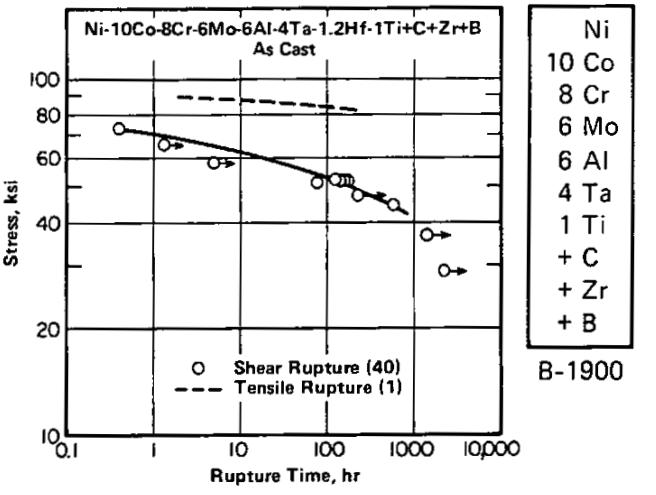


FIGURE 3.04241. SHEAR AND TENSILE RUPTURE STRENGTHS AT 1400 F (1,40)

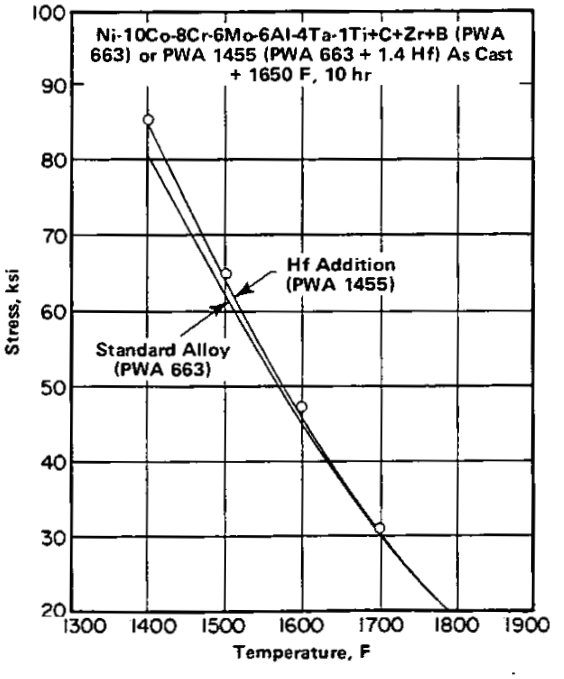


FIGURE 3.0431. EFFECT OF Hf ADDITION ON 300 HOUR CREEP RUPTURE CURVES (2)

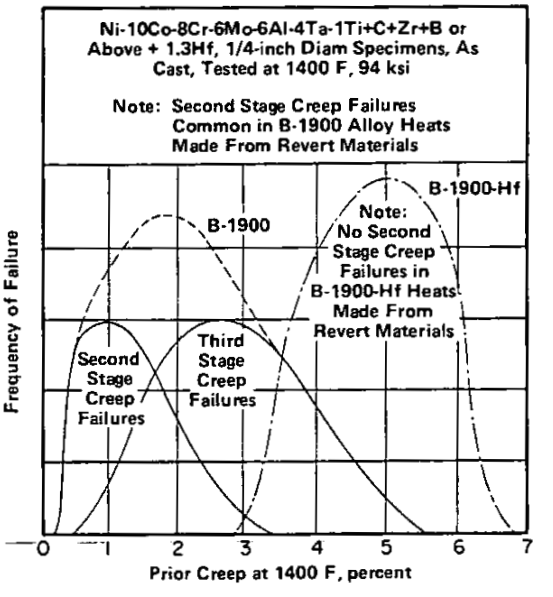


FIGURE 3.0432. FREQUENCY ANALYSIS OF B-1900 AND B-1900-Hf CREEP RUPTURE FAILURES (26,27)

Ni
10 Co
8 Cr
6 Mo
6 Al
4 Ta
1 Ti
+ C
+ Zr
+ B

B-1900

| Alloy | Ni-10Co-8Cr-6Mo-6Al-4Ta-1Ti+C+Zr+B or Ni-10Co-8Cr-6Mo-6Al-4Ta-1.37Hf-1Ti+C+Zr+B | | |
|---|---|---|---|
| Condition | As Cast | | |
| | B-1900 | | B-1900-Hf |
| Form | 1/4 Diam Cast to Size | 0.177 Diam From Cast Turbine Blade | 0.177 Diam From Cast Turbine Blade |
| 1400 F at 94 ksi | | | |
| Life, hours | 75 | 19 | 86 |
| Prior Creep, percent | 2.5 | 1.6 | 4.8 |
| 1800 F at 29 ksi | | | |
| Life, hours | 35 | 30 | 43 |
| Prior Creep, percent | 7 | 5 | 7 |

TABLE 3.0433. CREEP RUPTURE LIFE AND DUCTILITY OF AS-CAST SPECIMENS AND OF SPECIMENS MACHINED FROM CAST TURBINE BLADES OF STANDARD AND HAFNIUM-MODIFIED ALLOY (26,27)

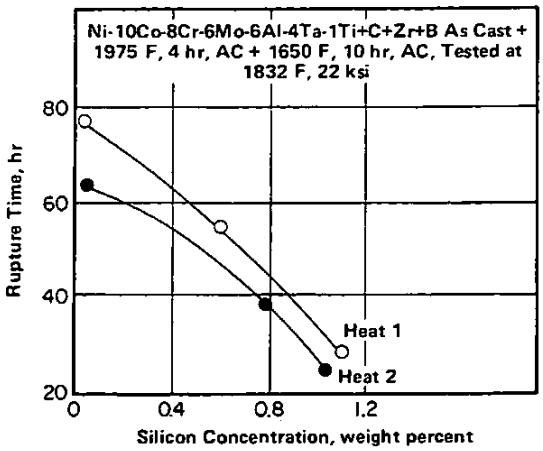


FIGURE 3.0434. EFFECT OF SILICON CONCENTRATION ON CREEP RUPTURE LIFE AT 22 KSI, 1832 F (28)

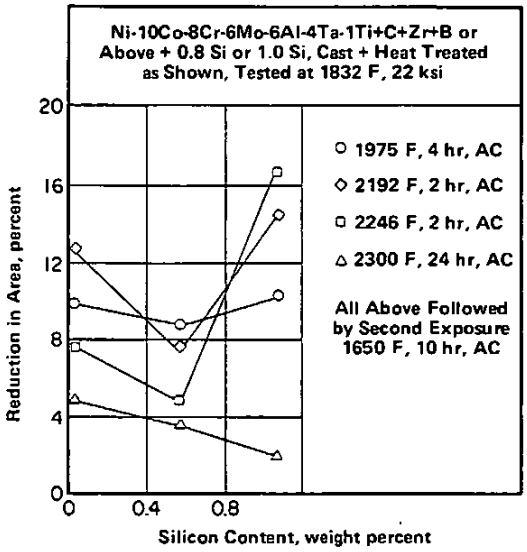


FIGURE 3.0435. EFFECT OF VARIOUS HEAT TREATMENTS AND SILICON CONTENT ON ~~RUPTURE DUCTILITY AT 1832 F,~~ 22 KSI (28)

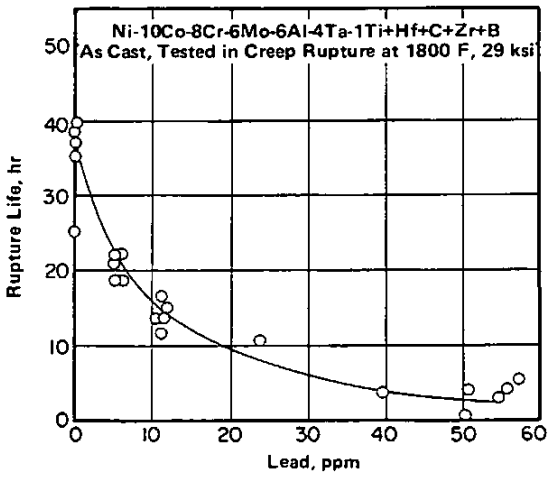


FIGURE 3.0436. EFFECT OF LEAD CONTENT ON CREEP RUPTURE LIFE AT 1800 F, 29 KSI (33)

| Ni |
|---|
| 10 Co |
| 8 Cr |
| 6 Mo |
| 6 Al |
| 4 Ta |
| 1 Ti |
| + C |
| + Zr |
| + B |

B-1900

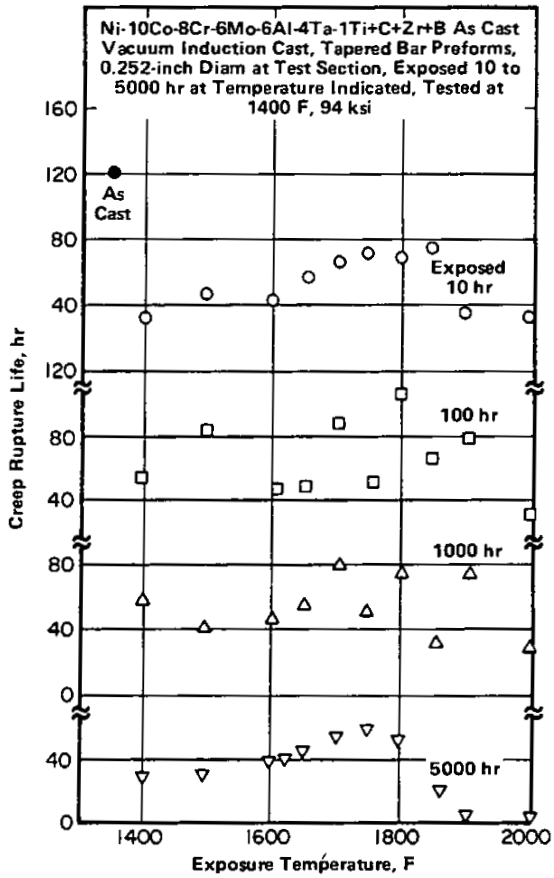


FIGURE 3.0441. EFFECT OF TIME AND TEMPERATURE OF EXPOSURE ON CREEP RUTPURE LIFE AT 1400 F, 94 KSI (21)

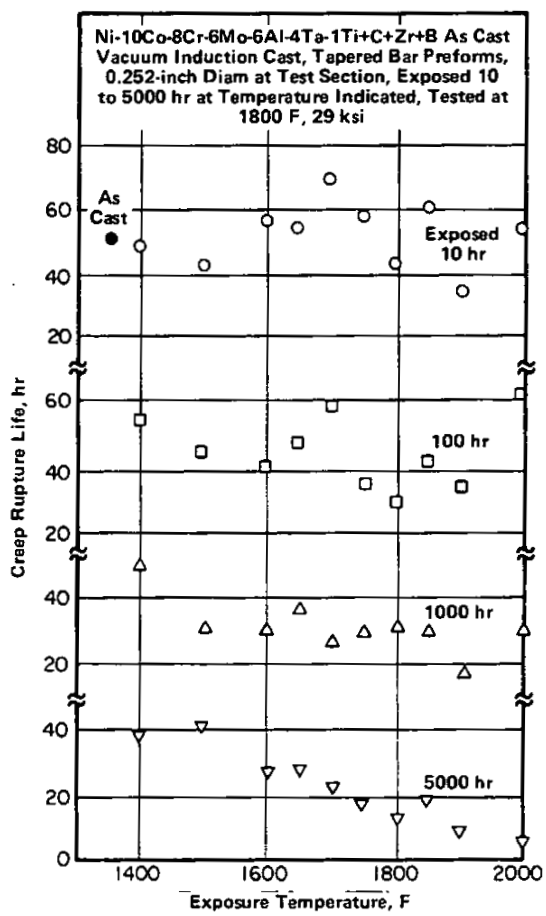


FIGURE 3.0442. EFFECT OF TIME AND TEMPERATURE OF EXPOSURE ON CREEP RUPTURE LIFE IN A SUBSEQUENT CREEP RUPTURE TEST AT 1800 F, 29 KSI (21)

Ni
10 Co
8 Cr
6 Mo
6 Al
4 Ta
1 Ti
+ C
+ Zr
+ B

B-1900

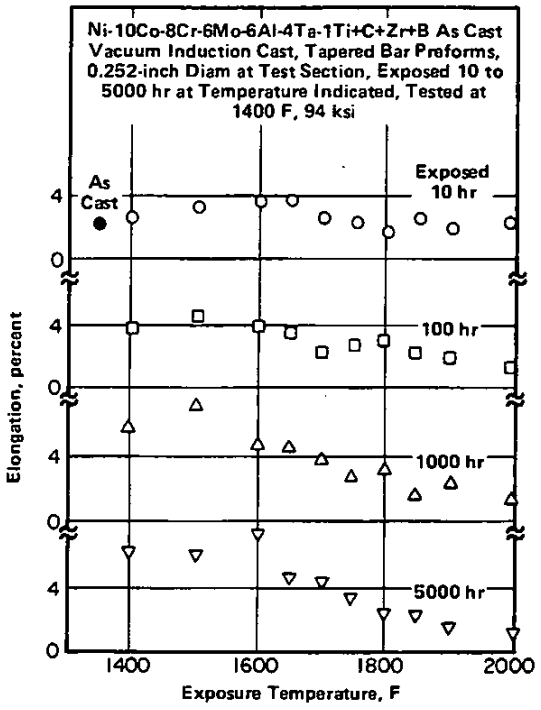


FIGURE 3.0443. EFFECT OF TIME AND TEMPERATURE OF PRIOR EXPOSURE ON DUCTILITY IN A SUBSEQUENT CREEP RUPTURE TEST AT 1400 F, 94 KSI (21)

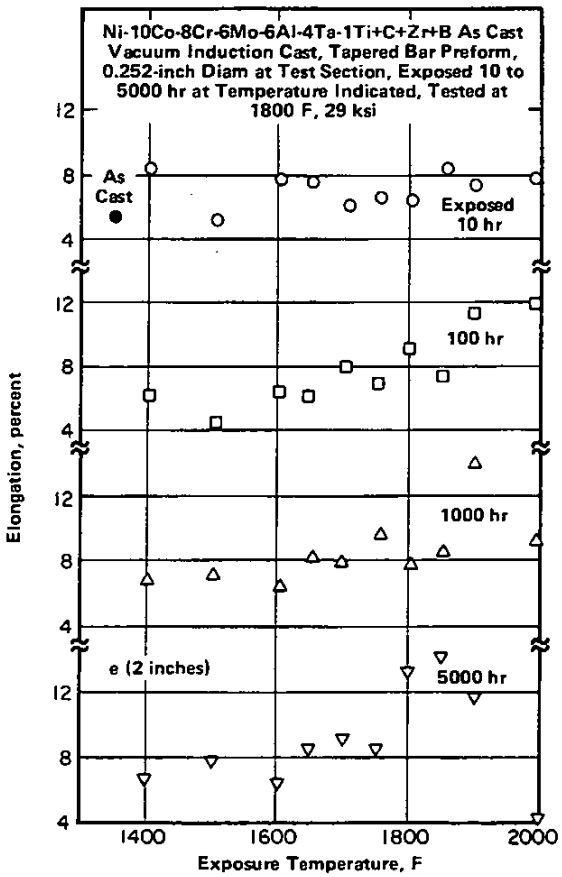


FIGURE 3.0444. EFFECT OF TIME AND TEMPERATURE OF PRIOR EXPOSURE ON DUCTILITY IN A SUBSEQUENT CREEP RUPTURE TEST AT 1800 F, 29 KSI (21)

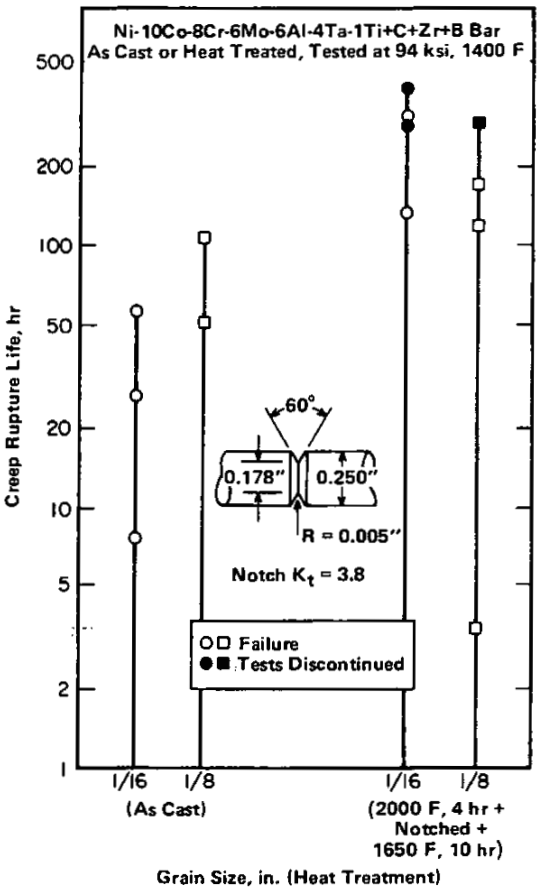


FIGURE 3.0451. EFFECT OF HEAT TREATMENT ON NOTCHED BAR CREEP RUPTURE LIFE AT 94 KSI, 1400 F FOR TWO GRAIN SIZES (2)

| Ni |
|---|
| 10 Co |
| 8 Cr |
| 6 Mo |
| 6 Al |
| 4 Ta |
| 1 Ti |
| + C |
| + Zr |
| + B |

B-1900

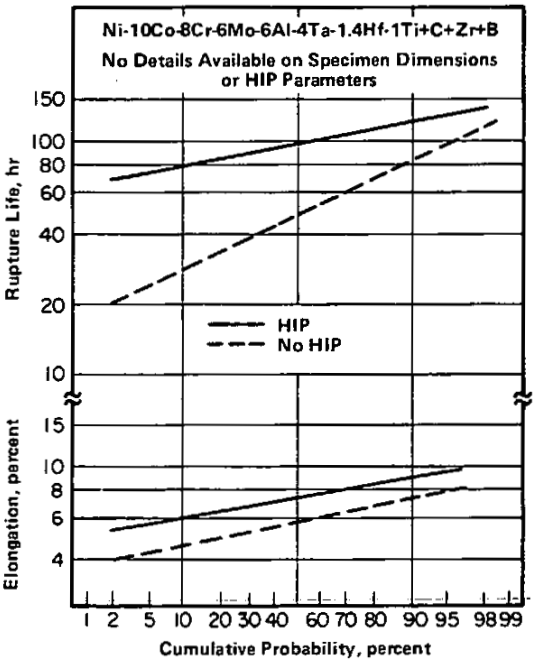


FIGURE 3.0461. EFFECT OF HIPING ON RUPTURE LIFE AND ELONGATION AT 1400 F, 94 KSI (41)

Ni
10 Co
8 Cr
6 Mo
6 Al
4 Ta
1 Ti
+ C
+ Zr
+ B

B-1900

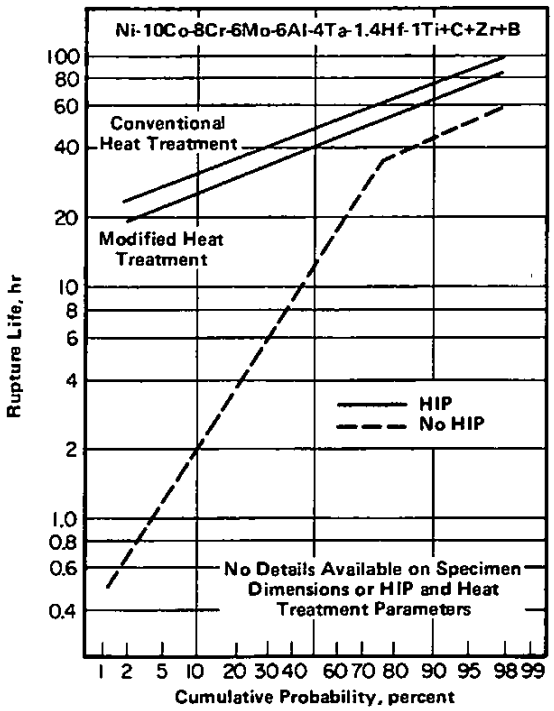


FIGURE 3.0462. EFFECTS OF HIPING AND HEAT TREATMENT ON RUPTURE LIFE AT 1800 F, AND 29 KSI OF THIN SECTION (0.030-INCH) ALLOY (41)

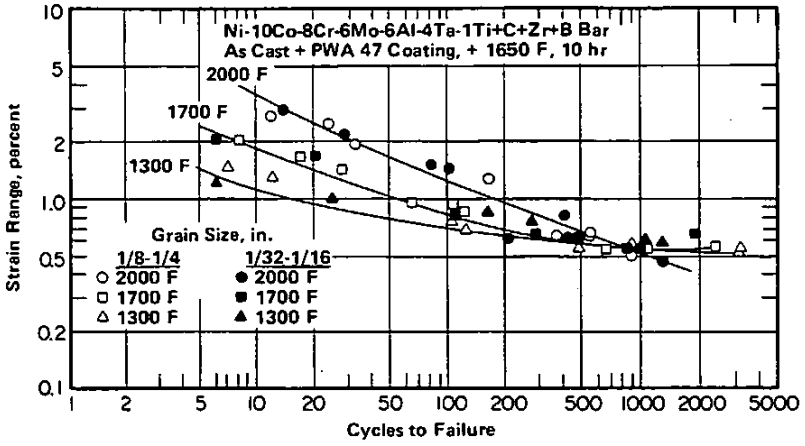


FIGURE 3.0511. STRAIN CONTROLLED LOW CYCLE FATIGUE AT 1300, 1700, AND 2000 F (2)

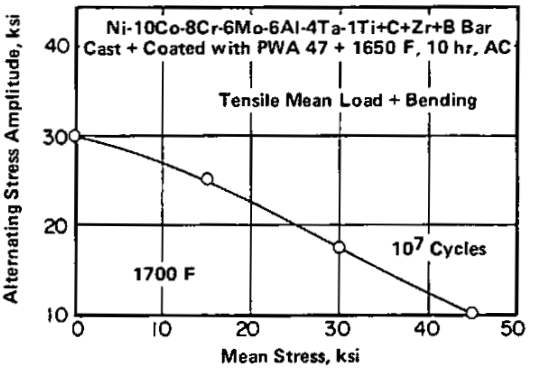


FIGURE 3.0512. MODIFIED GOODMAN DIAGRAM FOR $10^7$ CYCLES AT 1700 F (2)

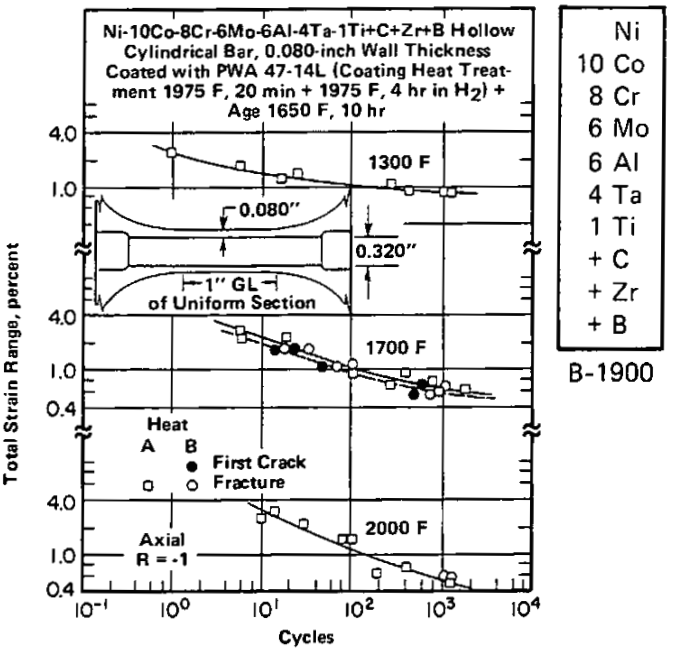


FIGURE 3.0513. LOW CYCLE FATIGUE CHARACTERISTICS OF SMOOTH HOLLOW SPECIMEN AT 1300, 1700, AND 2000 F IN STRAIN CONTROL (6)

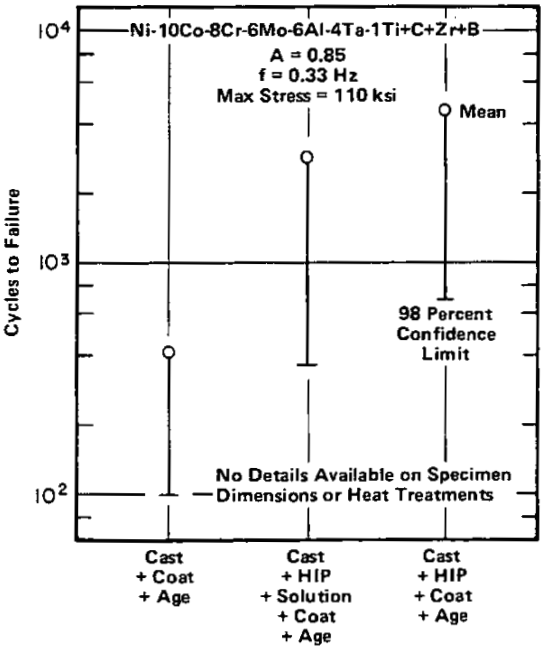


FIGURE 3.0514. EFFECT OF HIPING ON FATIGUE LIFE OF SMOOTH BAR AT 1400 F (43)

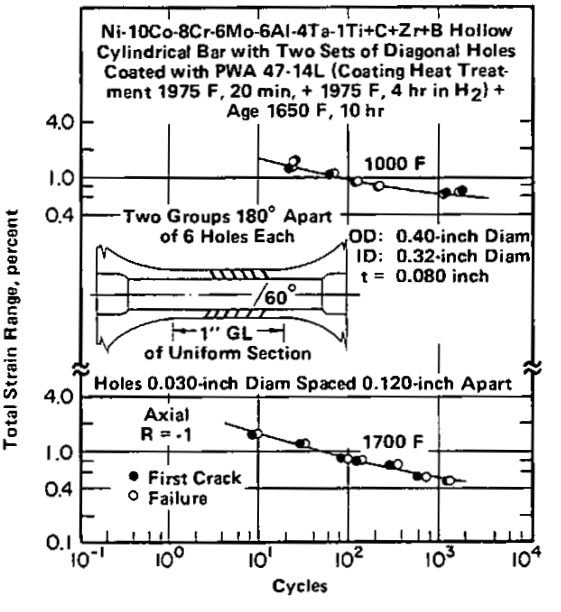


FIGURE 3.0521. LOW CYCLE FATIGUE CHARACTERISTICS AT 1000 AND 1700 F FOR TUBULAR SPECIMEN WITH TWO SETS OF DIAGONAL HOLES (6)

Ni
10 Co
8 Cr
6 Mo
6 Al
4 Ta
1 Ti
+ C
+ Zr
+ B

B-1900

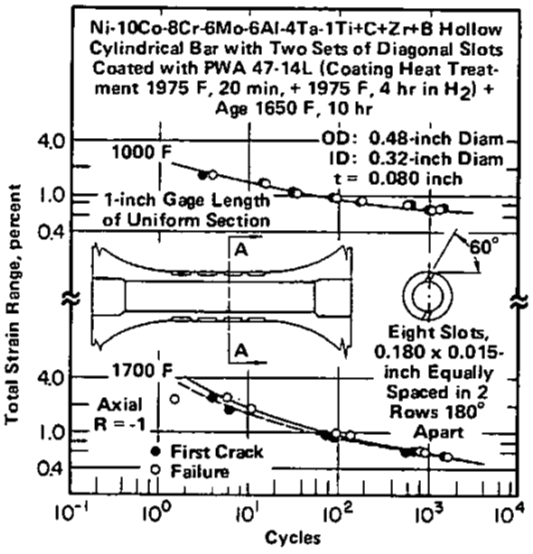


FIGURE 3.0522. LOW CYCLE FATIGUE CHARACTERISTICS AT 1000 AND 1700 F FOR TUBULAR SPECIMEN WITH TWO SETS OF DIAGONAL SLOTS (6)

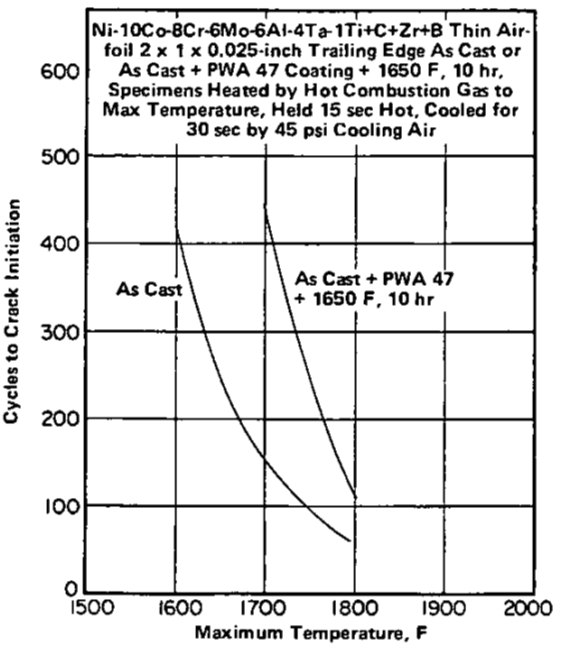


FIGURE 3.0531. THERMAL SHOCK RESISTANCE OF AIRFOIL IN AS-CAST AND IN COATED AND HEAT TREATED CONDITIONS (3)

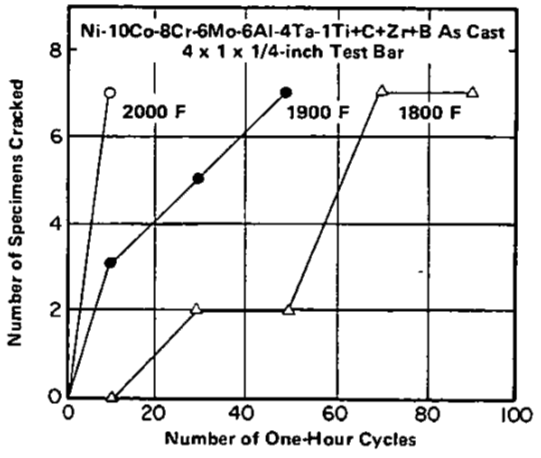


~~FIGURE 3.0532. THERMAL FATIGUE CRACK RESIS-~~ TANCE AT MAXIMUM TEMPERATURES OF 1800, 1900, AND 2000 F FOR AS-CAST ALLOY SAMPLES SUBJECTED TO HIGH VELOCITY OXIDATION CYCLING (7)

| Ni |
|---|
| 10 Co |
| 8 Cr |
| 6 Mo |
| 6 Al |
| 4 Ta |
| 1 Ti |
| + C |
| + Zr |
| + B |

B-1900

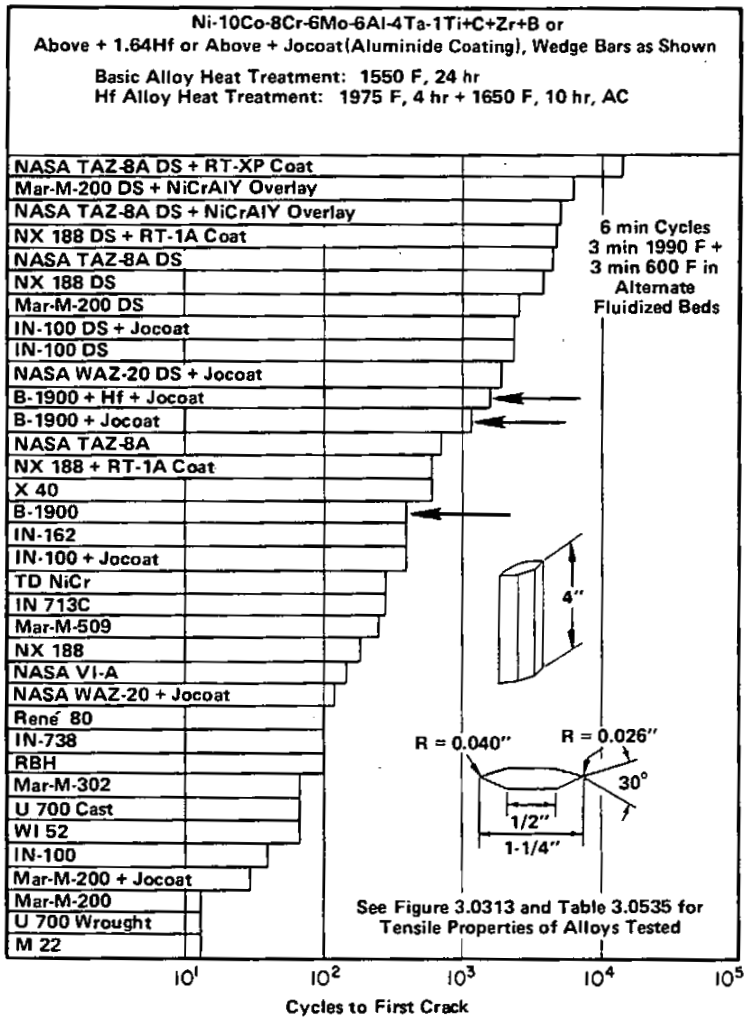


FIGURE 3.0533. THERMAL FATIGUE (CRACK INITIATION) IN ALTERNATE FLUIDIZED BEDS AT 600 AND 1990 F OF BASIC ALLOY, ALUMINIDE COATED ALLOY, AND ALLOY WITH HAFNIUM ADDITIONS, WITH COMPARISON TO OTHER SUPERALLOYS (31)

Ni
10 Co
8 Cr
6 Mo
6 Al
4 Ta
1 Ti
+ C
+ Zr
+ B

B-1900

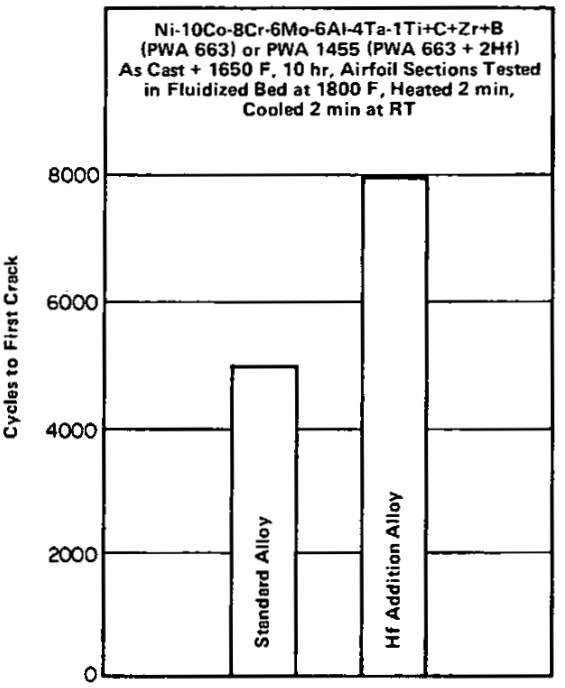


FIGURE 3.0534. EFFECT OF HAFNIUM ADDITIONS ON THERMAL FATIGUE RESISTANCE IN FLUIDIZED BED AT 1800 F (2)

| Alloy | Ni-10Co-8Cr-6Mo-6Al-4Ta-1Ti-+C+Zr+B or Ni-10Co-8Cr-6Mo-6Al-4Ta-1.64Hf+1Ti+C+Zr+B | |
|---|---|---|
| Condition | B-1900: 1550 F, 24 hr, AC<br>B-1900-Hf: 1975 F, 4 hr, AC + 1650 F, 4 hr, AC | |
| | B-1900 | B-1900-Hf |
| Mean Coeff Thermal Expansion, RT to 200 F, in./in./F | 6.5 | 6.5 |
| Thermal Conductivity at 200 F, Btu-in./ft$^2$-hr-F | 71 | 70 |
| Specific Gravity at RT | 8.22 | 8.28 |
| Proportional Limit at 1400 F, ksi | 136 | 102 |
| Ultimate Tensile Strength ($F_{tu}$) at 1400 F, ksi | 158 | 137 |
| Creep Rupture Life at 1800 F | | |
| at 25 ksi, hours | 99,95 | |
| at 24.5 ksi, hours | | 66,34 |
| Reduction of Area | | |
| Tensile Test at 1400 F, percent | 8 | 13 |
| Creep Test at 1800 F (As Above), percent | 11 | 13 |

TABLE 3.0535. SOME COMPARATIVE PROPERTIES OF BASIC ALLOY AND ALLOY WITH 1.64 PERCENT HAFNIUM (31)

Note: Lot used in fluidized bed thermal fatigue tests.

| |
|---|
| Ni |
| 10 Co |
| 8 Cr |
| 6 Mo |
| 6 Al |
| 4 Ta |
| 1 Ti |
| + C |
| + Zr |
| + B |

B-1900

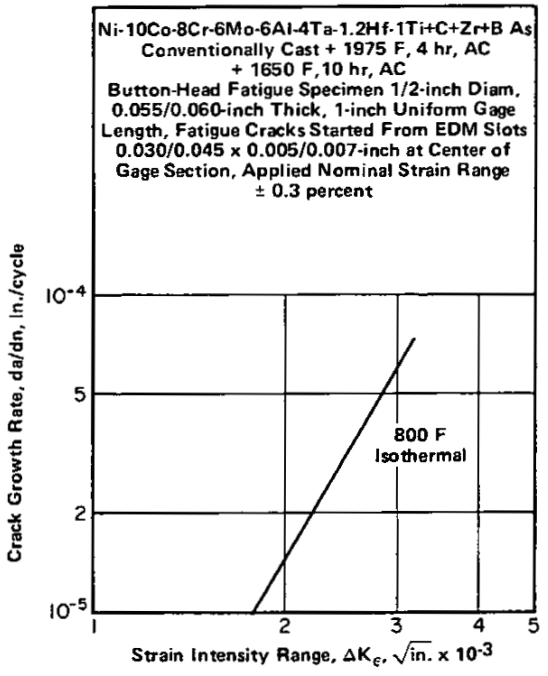


FIGURE 3.0541. CRACK PROPAGATION AT 800 F FOR ALLOY WITH HAFNIUM ADDITION (29)

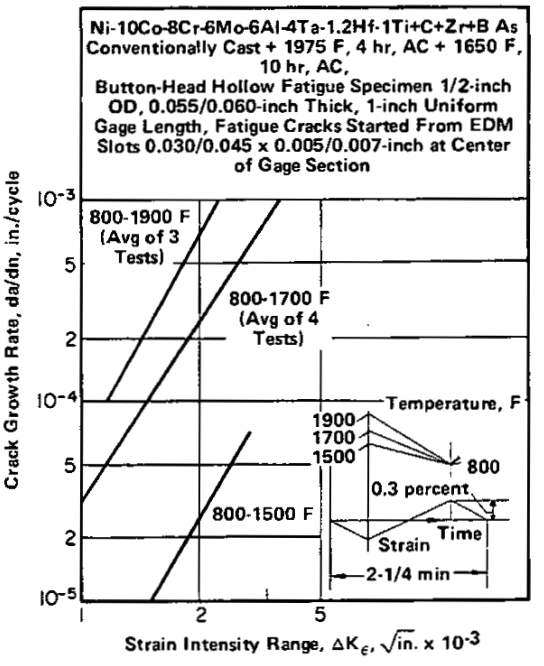


FIGURE 3.0542. CRACK PROPAGATION IN THERMO-MECHANICAL CYCLING OF ALLOY WITH HAFNIUM ADDITION (29,30)

Note: Mechanically imposed strain out of phase with temperature cycling.

Ni
10 Co
8 Cr
6 Mo
6 Al
4 Ta
1 Ti
+ C
+ Zr
+ B

B-1900

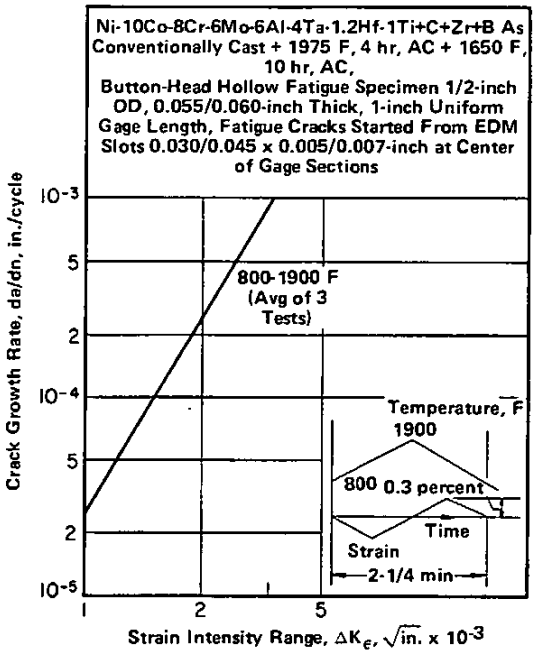


FIGURE 3.0543. PROPAGATION IN THERMOMECHANICAL CYCLING OF ALLOY WITH HAFNIUM ADDITION (29,30)

Note: Mechanically imposed strain in phase with temperature variation during half of cycle and out of phase in other half.

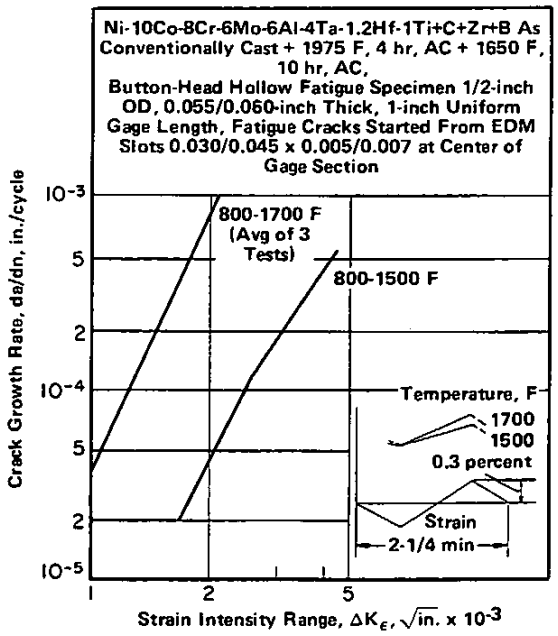


FIGURE 3.0544. CRACK PROPAGATION UNDER THERMOMECHANICAL CYCLING OF ALLOY WITH HAFNIUM ADDITION (29,30)

Note: Mechanically imposed strain in phase with temperature cycling.

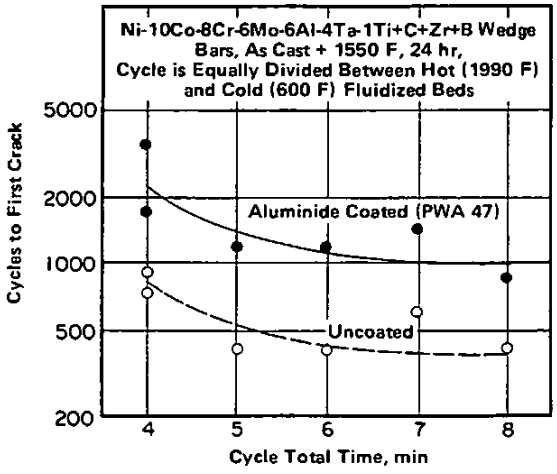


~~FIGURE 3.0551. EFFECT OF HEATING (AND EQUAL~~ COOLING) TIME ON CRACK INITIATION IN THERMAL FATIGUE OF BARE AND COATED SPECIMENS ALTERNATELY IMMERSED IN HOT AND COLD FLUIDIZED BEDS (11)

| |
|---|
| Ni |
| 10 Co |
| 8 Cr |
| 6 Mo |
| 6 Al |
| 4 Ta |
| 1 Ti |
| + C |
| + Zr |
| + B |

B-1900

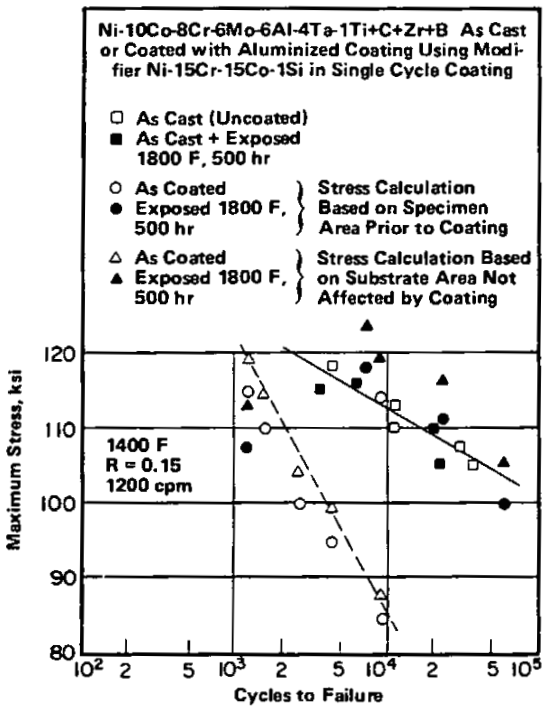


FIGURE 3.0552. LOW CYCLE FATIGUE AT 1400 F OF UNCOATED ALLOY AND OF ALLOY COATED BY A SINGLE HEATING CYCLE WITH AN ALUMINIZED COATING USING Ni-15Cr-15Co-1Si AS MODIFIER (22)

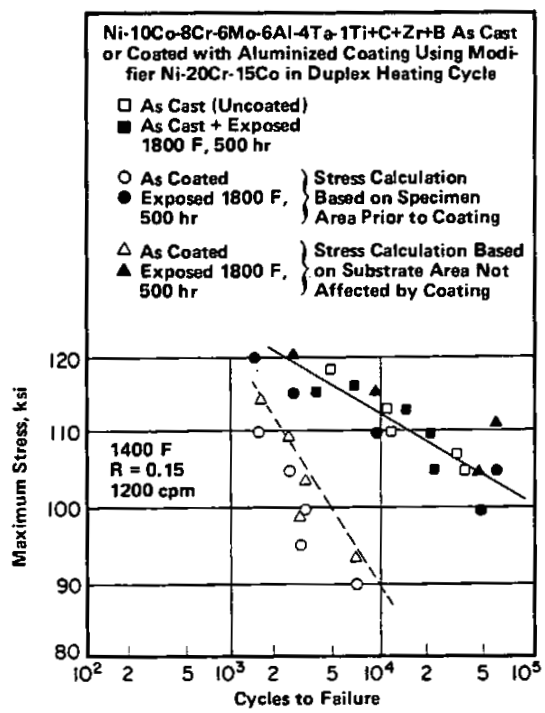


FIGURE 3.0553. LOW CYCLE FATIGUE AT 1400 F OF UNCOATED ALLOY AND OF ALLOY COATED BY A DUPLEX CYCLE WITH AN ALUMINIZED COATING USING Ni-20Cr-15Co AS MODIFIER (22)

Ni
10 Co
8 Cr
6 Mo
6 Al
4 Ta
1 Ti
+ C
+ Zr
+ B

B-1900

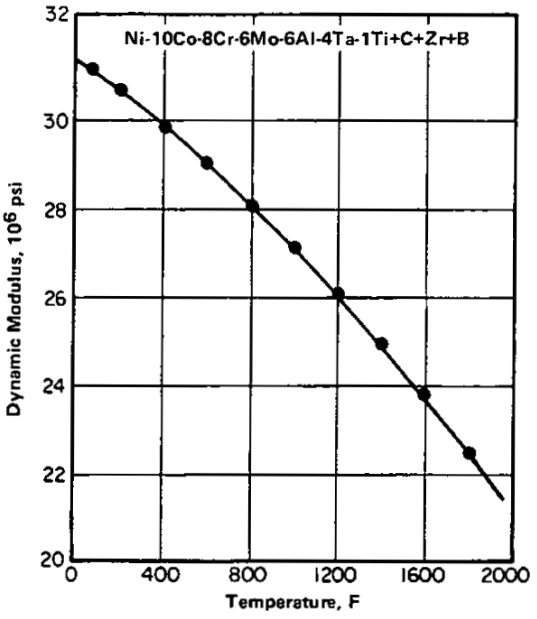


FIGURE 3.0621. DYNAMIC MODULUS OF ELASTICITY (4)

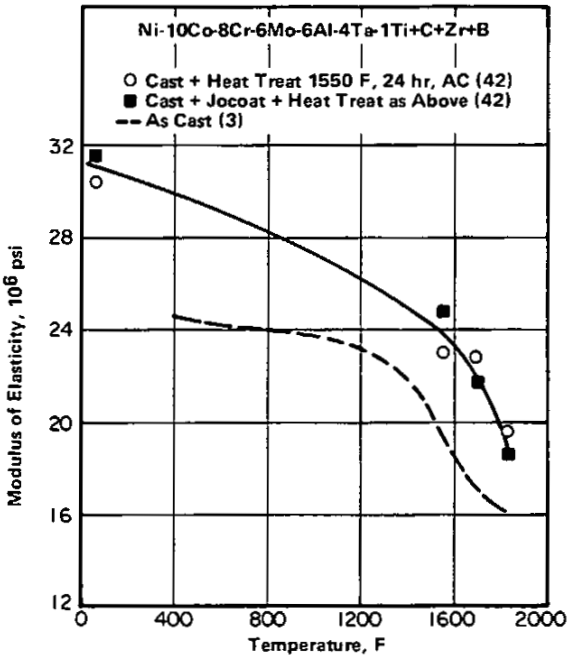


FIGURE 3.0622. STATIC MODULUS OF ELASTICITY (3,42)